The Astrophysical Journal, 853:15 (18pp), 2018 January 20 https://doi.org/10.3847/1538-4357/aaa3fc

Ages of the Bulge Globular Clusters NGC 6522 and NGC 6626 (M28) from *HST* Proper-motion-cleaned Color–Magnitude Diagrams*

L. O. Kerber[1,2], D. Nardiello[3,4], S. Ortolani[3,4], B. Barbuy[1], E. Bica[5], S. Cassisi[6], M. Libralato[3,4,7], and R. G. Vieira[1]
[1] Universidade de São Paulo, IAG, Rua do Matão 1226, Cidade Universitária, São Paulo 05508-900, Brazil; lokerber@uesc.br
[2] Universidade Estadual de Santa Cruz, DCET, Rodovia Jorge Amado km 16, Ilhéus 45662-000, Bahia, Brazil
[3] Università di Padova, Dipartimento di Astronomia, Vicolo dell'Osservatorio 5, I-35122 Padova, Italy
[4] INAF-Osservatorio Astronomico di Padova, Vicolo dell'Osservatorio 5, I-35122 Padova, Italy
[5] Universidade Federal do Rio Grande do Sul, Departamento de Astronomia, CP 15051, Porto Alegre 91501-970, Brazil
[6] Osservatorio Astronomico d'Abruzzo, Via M. Maggini sn., I-64100 Teramo, Italy
[7] Space Telescope Science Institute, 3700 San Martin Drive, Baltimore, MD 21218, USA
Received 2017 May 26; revised 2017 December 4; accepted 2017 December 20; published 2018 January 18

Abstract

Bulge globular clusters (GCs) with metallicities [Fe/H] $\lesssim -1.0$ and blue horizontal branches are candidates to harbor the oldest populations in the Galaxy. Based on the analysis of *HST* proper-motion-cleaned color–magnitude diagrams in filters F435W and F625W, we determine physical parameters for the old bulge GCs NGC 6522 and NGC 6626 (M28), both with well-defined blue horizontal branches. We compare these results with similar data for the inner halo cluster NGC 6362. These clusters have similar metallicities ($-1.3 \leqslant$ [Fe/H] $\leqslant -1.0$) obtained from high-resolution spectroscopy. We derive ages, distance moduli, and reddening values by means of statistical comparisons between observed and synthetic fiducial lines employing likelihood statistics and the Markov chain Monte Carlo method. The synthetic fiducial lines were generated using α-enhanced BaSTI and Dartmouth stellar evolutionary models, adopting both canonical ($Y \sim 0.25$) and enhanced ($Y \sim 0.30$–0.33) helium abundances. RR Lyrae stars were employed to determine the HB magnitude level, providing an independent indicator to constrain the apparent distance modulus and the helium enhancement. The shape of the observed fiducial line could be compatible with some helium enhancement for NGC 6522 and NGC 6626, but the average magnitudes of RR Lyrae stars tend to rule out this hypothesis. Assuming canonical helium abundances, BaSTI and Dartmouth models indicate that all three clusters are coeval, with ages between ∼12.5 and 13.0 Gyr. The present study also reveals that NGC 6522 has at least two stellar populations, since its CMD shows a significantly wide subgiant branch compatible with 14% ± 2% and 86% ± 5% for first and second generations, respectively.

Key words: globular clusters: general – globular clusters: individual (NGC 6522, NGC 6626, NGC 6362)

1. Introduction

The bulk of the Milky Way (MW) bulge stars show a lower-metallicity end at $-1.5 \lesssim$ [Fe/H] $\lesssim -1.0$ (e.g., Rojas-Arriagada et al. 2014, 2017; Zoccali et al. 2017, and references therein). These relatively high lower-end metallicities are expected from an early fast chemical enrichment in the central parts of the Galaxy, as modeled by, e.g., Cescutti et al. (2008). From a selection of bulge globular clusters (GCs) presented by Bica et al. (2016), it was shown that their metallicity distribution also has a peak at [Fe/H] ~ -1.0. A subclass of these clusters show a blue horizontal branch (BHB), making these combined characteristics indicative, in principle, of a very old age (Lee et al. 1994). Furthermore, Marín-Franch et al. (2009) demonstrated that the GCs with galactocentric distance (R_{GC}) less than 10 kpc follow a flat age–metallicity relation with an age dispersion of only ∼5%, reinforcing the idea that a very low metallicity is not a restrictive prior condition to find stellar relics in the bulge.

Our main targets in this work, NGC 6522 and NGC 6626 (M28), are both bulge GCs with similar metallicities ($-1.3 \leqslant$ [Fe/H] $\leqslant -1.0$) and BHBs and are both affected by field contamination and high absorption ($A_V > 1.20$) due to their proximity to the Galactic center ($R_{GC} < 3$ kpc). In particular, NGC 6522 is a very interesting GC located in Baade's Window. Located at a galactocentric distance $\lesssim$1 kpc, likely in the foreground with respect to the Galactic center, NGC 6522 was suggested to be among the oldest clusters in the MW (Barbuy et al. 2009).

An important issue in the analysis of stellar populations in GCs is the presence of multiple stellar populations (e.g., Milone et al. 2015, 2017; Nardiello et al. 2015a, 2015b; Piotto et al. 2015). In this paper we address this point with optical *Hubble Space Telescope* (*HST*) bands, and we present the first photometric evidence for multiple stellar populations in NGC 6522.

Based on *VLT*/FLAMES[8] optical high-resolution spectroscopy, Barbuy et al. (2009, 2014) and Ness et al. (2014) analyzed NGC 6522 and derived its metallicity and chemical abundances. With the same instrument, Villanova et al. (2017) performed a similar analysis for NGC 6626 and interestingly found the presence of at least two stellar populations in the cluster. Very recently, using near-infrared high-resolution spectroscopy from the APOGEE (Apache Observatory Galactic Evolution Experiment; Majewski & APOGEE Team and APOGEE-2 Team 2016), Schiavon et al. (2017) discovered one star in NGC 6522 with a very high nitrogen abundance ([N/Fe] $= +1.04$), suggesting that this cluster hosts multiple stellar populations. An additional three stars analyzed by J. G. Fernández-Trincado et al. (2018, in preparation) were found with similar chemical abundances.

* Based on observations with the NASA/ESA *Hubble Space Telescope*, obtained at the Space Telescope Science Institute.

[8] Fibre Large Array Multi Element Spectrograph (FLAMES) is the multi-object, intermediate- and high-resolution spectrograph of the Very Large Telescope (VLT).

Furthermore, Recio-Blanco et al. (2017) inferred a high Al abundance together with a low Mg abundance for one star, corroborating the hypothesis of more than one stellar population hosted by NGC 6522.

Despite the accurate metallicity and chemical abundance determinations for NGC 6522 and NGC 6626, to date there are no analogous results for self-consistent age, distance, and reddening determinations for these clusters. The main reason is the lack of deep, proper-motion-cleaned color–magnitude diagrams (CMDs), based on high-photometric-precision data with which to perform a statistical analysis. Currently only the *HST* (e.g., Ortolani et al. 2007; Piotto et al. 2015; Ferraro et al. 2016) and 8 m class telescopes with multi-conjugated adaptive optical (MCAO) systems (e.g., Ferraro et al. 2009; Saracino et al. 2015, 2016) are able to collect images with such high quality for GCs, spatially resolving stars with an FHWM $\lesssim 0.10$ arcsec in their cores. The primary goal of this work is to derive such physical parameters (age, distance, and reddening) for NGC 6522 and NGC 6626 using a statistical isochrone fitting on accurate, proper-motion-cleaned *HST*-based CMD.

These two clusters were not included in the ACS Survey of GCs (Sarajedini et al. 2007) or in the *HST* UV Legacy Survey of Galactic GCs (Piotto et al. 2015), and consequently they were not listed in the most recent and comprehensive papers concerning dating Galactic GCs (De Angeli et al. 2005; Marín-Franch et al. 2009; Dotter et al. 2010; VandenBerg et al. 2013; Wagner-Kaiser et al. 2016, 2017). Although they are included in the large compilation of age, metallicity, and abundance pattern for 41 Galactic GCs presented by Roediger et al. (2014), their ages (15.0 ± 1.10 for NGC 6522 and 14.0 ± 1.1 for NGC 6626) are marked as "less certain" values.

The only two age determinations for NGC 6522 based on *HST* data were carried out by Meissner & Weiss (2006) and Barbuy et al. (2009), in both cases using the same *HST*/WFPC2[9] data in F439W and F555W bands collected in a snapshot program (Piotto et al. 2002). Since the CMDs generated with these data barely reach 1 mag below the main-sequence turnoff (MSTO), the most solid results in these papers were based on the magnitude difference between the MSTO and the horizontal branch (HB) ($\Delta V_{\rm TO}^{\rm HB}$). In fact, NGC 6522 presented a remarkably high $\Delta V_{\rm TO}^{\rm HB}$ value, suggesting that it is $\sim$2 Gyr older than 47 Tuc and M5 (NGC 5904) when the mean loci of these clusters are overplotted (Barbuy et al. 2009). Using the same stellar evolutionary models (A Bag of Stellar Tracks and Isochrones—BaSTI; Pietrinferni et al. 2004), Meissner & Weiss (2006) recovered an age between 13.9 and 16.1 Gyr, whereas Barbuy et al. (2009) estimated $\sim$16 Gyr.

As concerns NGC 6626, Testa et al. (2001) presented a relative age determination based on *HST*/WFPC2 data. These authors analyzed the F555W, F555W–F814W CMD for this cluster in comparison with three halo GCs with BHB (NGC 2298, NGC 5897, NGC 6535) whose metallicities are [Fe/H] ~ -1.73, -1.70, and -1.83, respectively, i.e., about 0.4–0.5 dex lower than the value for NGC 6626 ([Fe/H] ~ -1.33). Measuring the color difference between the MSTO and an arbitrary point in the red giant branch (RGB), they identified NGC 6626 as the oldest cluster in their sample, 1.2 ± 0.9 Gyr older than NGC 2298 and 2.4 ± 1.6 Gyr older than NGC 6535. Assuming an age of $\sim$13.0 Gyr for these two clusters as determined by Dotter et al. (2010), NGC 6626 could be older than $\sim$14.0 Gyr.

In order to determine some of the main physical parameters of NGC 6522 and NGC 6626 in a comparative way, we retrieved *HST*/ACS[10] archive images in filters F435W and F625W for these clusters. Additional *HST*/WFPC2 archive images for each cluster allowed us to generate proper-motion-cleaned CMDs, drastically minimizing the effect of the field stellar contamination in our results. The main method employed in the present work is based on statistical comparisons between observed and synthetic fiducial lines, providing ages, distance moduli, and reddening values self-consistently. We used α-enhanced BaSTI and Dartmouth isochrones with canonical ($Y \sim 0.25$) and enhanced helium abundance ($Y = 0.30$ for BaSTI; $Y = 0.33$ for Dartmouth) to generate the synthetic fiducial lines. The MSTO magnitude and the HB level are independently determined in order to give additional tests to better constrain the cluster physical parameters. In particular, the RR Lyrae stars presented in the compilation by Clement et al. (2001) (hereafter referred to as Clement's catalog—2017 edition[11]) and in the OGLE catalog[12] (Soszyński et al. 2014) were used to determine the HB magnitude level. Further detailed studies of the HB morphology in these clusters will be addressed in a future work.

For comparison purposes, we included the analysis of NGC 6362, a GC that has been extensively studied in the aforementioned *HST* surveys and for which there are *HST*/ACS archive images in the F625W and F438W filters. It is an inner halo GC ($R_{\rm GC} = 5.1$ kpc) located at a moderate Galactic latitude ($\sim 17\overset{\circ}{.}6$) and therefore toward a region with low reddening ($E(B-V) \lesssim 0.10$) and low field stellar contamination. Its metallicity was recently determined by means of high-resolution spectroscopy ([Fe/H] $= -1.09 \pm 0.01$, Mucciarelli et al. 2016; [Fe/H] $= -1.07 \pm 0.01$; Massari et al. 2017), confirming NGC 6362 to be similar in metallicity to NGC 6522 and NGC 6626. On the other hand, differently from NGC 6522 and NGC 6626, NGC 6362 shows a red horizontal branch (RHB).

Furthermore, other works based on *HST* data (Dalessandro et al. 2014; Piotto et al. 2015; Milone et al. 2017) and high-resolution spectroscopy (Mucciarelli et al. 2016) demonstrated that NGC 6362 hosts multiple stellar populations. Since NGC 6362 is one of the analyzed clusters in De Angeli et al. (2005), Meissner & Weiss (2006), Marín-Franch et al. (2009), Dotter et al. (2010), Paust et al. (2010), VandenBerg et al. (2013), and Wagner-Kaiser et al. (2016, 2017), it is a key comparison object for the present paper. It was identified as one of the oldest Galactic GCs by Marín-Franch et al. (2009), Paust et al. (2010), VandenBerg et al. (2013), and Wagner-Kaiser et al. (2016, 2017).

The observations, proper-motion cleaning, and radial density profiles are described in Section 2. CMDs are presented in Section 3. In Section 4 the literature metallicities and abundances are reported. In Section 5 the isochrone fitting method is presented, and adopted stellar evolutionary models are briefly described. In Section 6 cluster ages, distances, and reddening values are derived. In Section 7 a discussion and a tentative identification of multiple stellar populations in the

[9] Wide Field and Planetary Camera 2 (WFPC2).

[10] Advanced Camera for Surveys (ACS).

[11] http://vizier.cfa.harvard.edu/viz-bin/VizieR?-source=V/150

[12] http://ogledb.astrouw.edu.pl/~ogle/CVS/

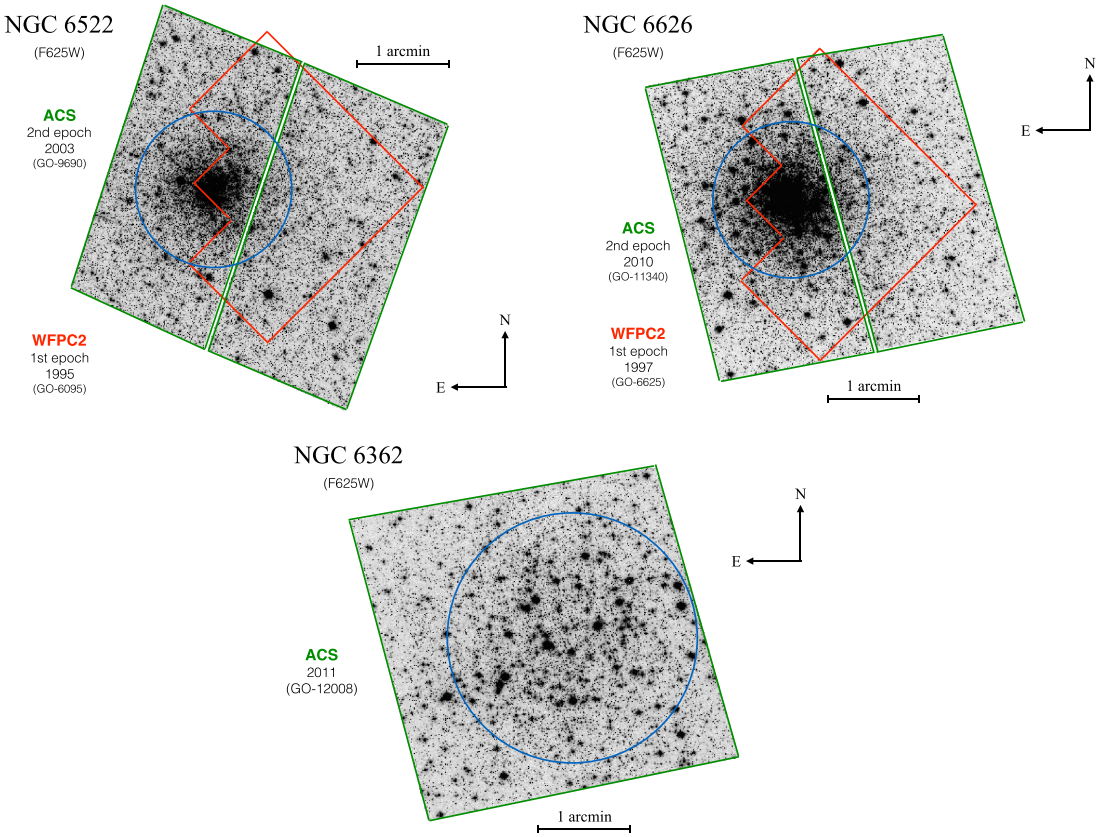

Figure 1. *HST* images of the GCs NGC 6522 (left), NGC 6626 (right), and NGC 6362 (middle). All these images were collected with ACS/WFC in the F625W filter. North is up, east is left. The ACS/WFC field of view is 202 × 202 arcsec^2. The red contours correspond to the WFPC2 field of view of the first epoch for NGC 6522 and NGC 6626, whereas the blue circles are the adopted limiting radius defining the bulk of the cluster's stars.

sample clusters are presented. Conclusions are drawn in Section 8.

2. Observations and Data Reduction

HST images of the bulge GCs NGC 6522 and NGC 6626 and the inner halo cluster NGC 6362 are employed in the present work (Figure 1). In order to build proper-motion-cleaned CMDs for the first two clusters, images from two different epochs were retrieved from the *HST* archive.[13]

The *HST* images of NGC 6522 were collected as part of the program GO-9690 (PI: J. Grindlay), with the ACS/WFC.[14] The observations of NGC 6626 were performed using the same camera during the program GO-11340 (PI: J. Grindlay). For both clusters we reduced the data in F435W, F625W, and F658N filters. For NGC 6362 we employed data in F438W obtained with the WFC3/UVIS[15] and in F625W (ACS/WFC) collected during GO-13297 (PI: G. Piotto) and GO-12008 (PI: A. Kong), respectively.

As a first step, all images were corrected for the imperfect charge transfer efficiency. The data reduction was carried out using the software described in detail by Anderson et al. (2008). The point-spread function (PSF) model used in this work is a perturbation of the library PSF by Anderson & King (2006); in this way, we took into account the change of focus of the spacecraft. We corrected the measured stellar positions for geometric distortion by using the solution provided by Anderson & King (2006). We calibrated the magnitudes into the Vega-mag systems as in Bedin et al. (2005). Finally, we corrected the CMDs for differential reddening using the procedure described in detail by Milone et al. (2012).

An inspection of the theoretical magnitude predictions in filters F438W and F435W indicates a negligible difference of ∼0.01 mag. Even if small, this small difference was taken into account when the F435W magnitudes of NGC 6362 were converted to the F438W filter.

For NGC 6522 we used as first-epoch images in F439W and F555W taken with the WFPC2 as part of the program GO-6095 (PI: S. Djorgovski) on 1995 September 9 ($t_{\rm I} = 1995.69$). As second epoch we used all the images in F435W, F625W, and F658N taken during GO-9690 (PI: J. Grindlay) on 2003 July 10 ($t_{\rm II} = 2003.52$). The time baseline for the proper-motion measurements is ∼7.83 yr. For NGC 6626 we considered as first epoch the WFPC2 observations in F555W and F814W carried out during GO-6625 (PI: R. Buonanno) on 1997 September 12 ($t_{\rm I} = 1995.70$), while as second epoch we used the F435W and F625W observations taken for GO-11340 (PI: J. Grindlay) on 2010 April 26 ($t_{\rm II} = 2010.32$). The time baseline is ∼14.62 yr.

2.1. Proper Motions

Stellar relative proper motions were measured for NGC 6522 and NGC 6266, in order to separate cluster members and field stars. The approach used is the same as that by, e.g., Anderson et al. (2006), Bellini et al. (2010), Libralato et al. (2014), and Nardiello et al. (2016).

[13] https://archive.stsci.edu
[14] Wide Field Channel (WFC) on the ACS.
[15] UVIS Channel on the Wide Field Camera 3 (WFC3).

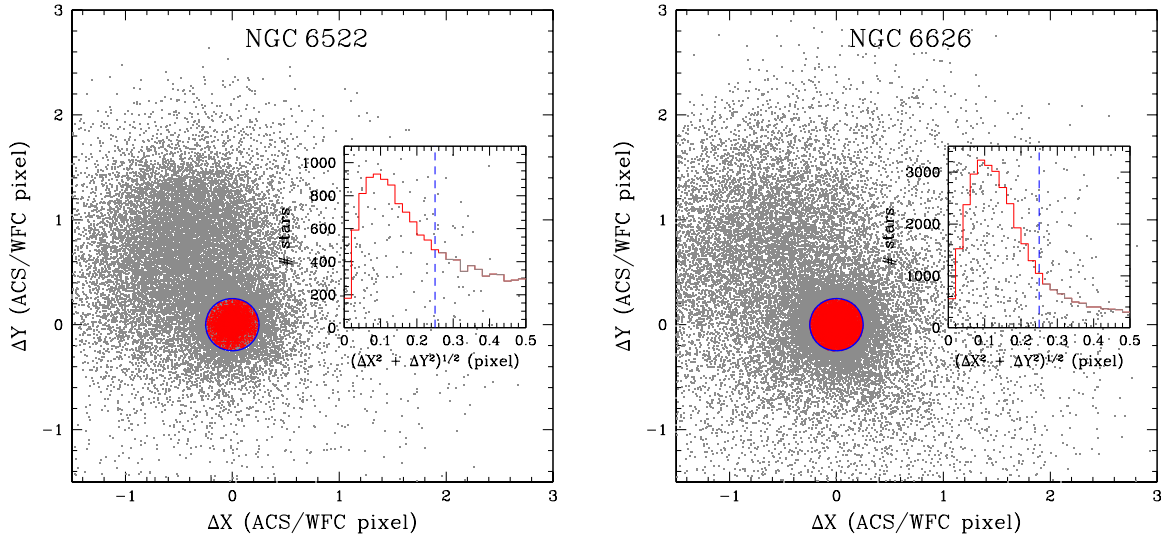

Figure 2. VPD of NGC 6522 (left) and NGC 6626 (right). Likely cluster stars (red) and remaining stars (gray) are presented in each panel. The histograms inserted in insets give the number of stars as a function of $(\Delta X^2 + \Delta Y^2)^{1/2}$. The vertical dashed line represents the cutoff limit to define the cluster members.

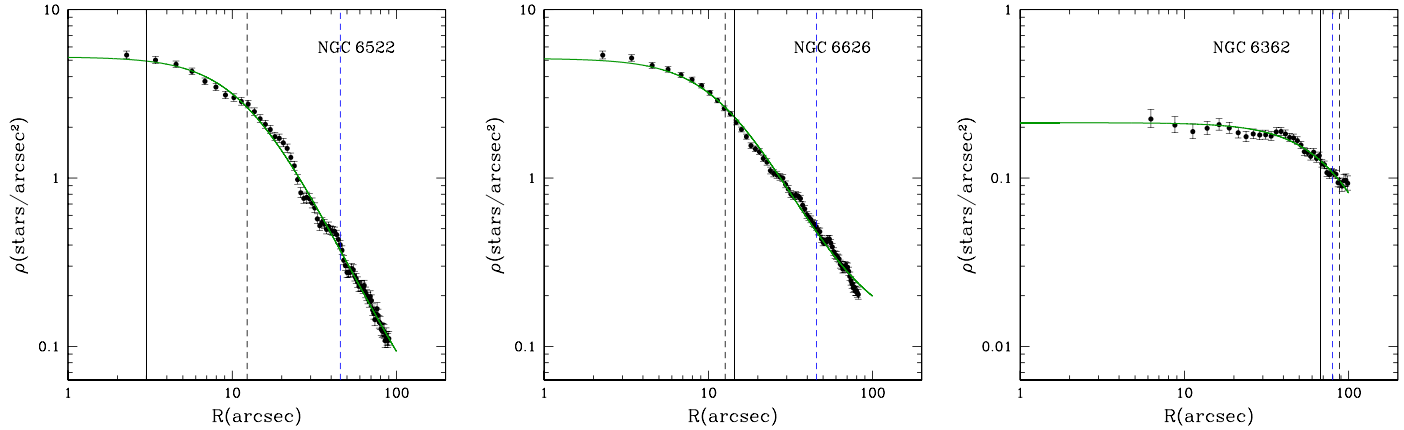

Figure 3. Radial density profile of NGC 6522 (left), NGC 6626 (middle), and NGC 6362 (right). The best fits for the King model are also presented (green lines). Vertical lines correspond to limiting radius as shown in Figure 1 (blue dashed line), core radius from King's model (black dashed line), and core radius from Trager et al. (1995; black solid line).

Briefly, we used six-parameter, local linear transformations to transform stars' positions as measured in the first-epoch reference frame into that of the second epoch and then computed the displacements. To compute the coefficients of these local transformations, we considered a sample of close-by, likely cluster members (e.g., red giant branch [RGB] and subgiant branch [SGB] stars). These stars were selected according to their location in the CMDs and/or in the vector-point diagram (VPD). By using cluster stars, the stellar displacements in both coordinates (ΔX, ΔY) are computed relative to the cluster mean motion, and in the VPD the cluster distribution is centered at (0,0), while the bulk of the field stars are located in a different region (Figure 2). In this figure the number of stars as a function of total displacements $(\Delta X^2 + \Delta Y^2)^{1/2}$ is shown in the insets within each of the two main panels. The cutoff in proper motion was chosen based on the visual inspection of the final cleaned CMDs.

2.2. Radial Density Profiles

The radial density profiles of NGC 6522, NGC 6626, and NGC 6362 are presented in Figure 3.

They were determined by counting stars in a sequence of concentric rings using the F625W photometric catalog. The center of the clusters was inferred by changing the center position until we found the (X, Y) coordinates where the density maximizes. The area of each ring was evaluated by means of a numerical approach, where a large number of artificial points are generated in random positions. Those points located inside the boundaries of the *HST* instruments (overlapping WFPC2 and ACS field of view for NGC 6522 and NGC 6626; ACS for NGC 6362) (see Figure 1) are used to determine the area fraction covered by them. Only cluster stars brighter than $\mathrm{F625W_{MSTO}} + 1.0$ mag were used, preventing incompleteness effects. In order to determine the core radius (r_c) and the central star density (ρ_0), we adopted the two-parameter model from King (1962):

$$\rho(r) = \rho_0 \frac{1}{1 + \left(\frac{r}{r_c}\right)^2}.$$

A nonlinear minimum square fitting was employed to find the best solutions. The structural parameters from these fits are shown

Table 1
Coordinates and Present Structural Parameters

Cluster	R.A. (J2000) (h m s)	Decl. (J2000) (° ′ ″)	l (deg)	b (deg)	ρ_0 (stars/arcsec^2)	r_c (arcsec)
NGC 6522	18:03:34.08	−30:02:02.3	−1.02	−3.93	5.22 ± 0.13	12.32 ± 0.26
NGC 6626 (M28)	18:24:32.89	−24:52:11.4	7.80	−5.58	5.01 ± 0.14	12.67 ± 0.31
NGC 6362	17:31:54.99	−67:02:54.0	325.55	−17.57	0.233 ± 0.026	91.2 ± 11.9

Note. F625W magnitude cutoff for the King's model: $F625W_{MSTO}$ + 1.0 (see Table 2).

in Table 1. NGC 6522 and NGC 6626 have very similar and small core radii (∼12 arcsec), as well as similar and high central star density (∼5 stars arcsec^{-2}), different from the ones presented for NGC 6362 (91 ± 12 arcsec and 0.23 ± 0.03 stars arcsec^{-2}). In Figure 3 we compare the core radius recovered by us and the ones determined by Trager et al. (1995). The agreement is very good for NGC 6626 and NGC 6362. On the other hand, we obtained a core radius for NGC 6522 significantly larger than the one determined by Trager et al. (1995).

We did not apply the three-parameter King's model since the observed angular radii covered by the *HST* images (∼2 arcmin) are significantly smaller than the tidal radii of these clusters (≳5 arcmin). In particular, only the core region of NGC 6362 was analyzed because it is a very extended cluster with a core radius ≳60 arcsec. For the two bulge clusters the analyzed area corresponds to about 10 times the core size.

3. Color–Magnitude Diagrams

Figure 4 shows the CMDs of NGC 6522, NGC 6626, and NGC 6362. In all CMDs, the main sequence (MS), SGB, and RGB are very well defined after field star decontamination, ranging along at least 7 mag. Different magnitude and color limits are adopted for each cluster in order to place their MSTO level side by side, thus allowing direct comparisons. An important difference between these clusters is related to the HB: NGC 6522 and NGC 6626 have similar BHBs, whereas NGC 6362 presents an RHB. Looking at Figure 4, it seems that the stars in the upper RGB are significantly more scattered in the two bulge GCs than in NGC 6362, indicating that there is a possible saturation effect for stars brighter than the HB. Blue stragglers seem to be present in the three clusters.

Figure 4 also presents the fiducial line for each cluster, defined by the color median throughout the MS, SGB, and RGB, using magnitude bins of Δmag = 0.15.

3.1. MSTO

The MSTO, defined as the bluest MS point, is the main CMD feature to characterize ages of stellar clusters. In this work the MSTO point was determined by adopting the following procedure. A denser sequence of fiducial points was determined by applying small magnitude shifts (0.01 mag) to the original magnitude bins (0.15 mag), therefore better sampling the MSTO region and reducing the uncertainties in the MSTO position. The final MSTO magnitude in the F625W filter was defined as the average over all fiducial points with a color difference ⩽0.010 mag (∼random uncertainty in color for each point) relative to the bluest point, with the uncertainty in this value being provided by the standard deviation over these points (⩽0.08 mag for all clusters). These determinations are presented in Table 2.

3.2. HB Level and RR Lyrae Stars

For BHB clusters the HB magnitude at the RR Lyrae position is uncertain, particularly at the TO color, where the HB presents few or even no stars, as can be seen in Figure 4. For this reason the use of RR Lyrae to determine the HB magnitude in BHB clusters is highly recommended, sometimes mandatory (Zoccali et al. 1999).

To provide a first guess about the location of the RR Lyrae stars in the *HST* CMDs, we cross-matched our *HST* data with the RR Lyrae stars presented in Clement's catalog. We identified five RR Lyrae in NGC 6522 and seven in NGC 6626 and NGC 6362 (Figure 4). Although most of these RR Lyrae stars were not present in our multi-epoch photometry, preventing their membership evaluation, they appear to be cluster members owing to their magnitudes, similar to the HB one. As expected, significant magnitude and color spreads can be seen in the *HST* photometry for these short-period variable stars. This is an effect of instantaneous measurements at random phase positions in RR Lyrae light curves, since they present amplitudes that can reach ∼1.0 mag in optical bands and periods of ∼0.2–0.7 days.

In order to reduce the uncertainties in the HB level that would be introduced by determinations using instantaneous magnitudes, we analyzed the V mean magnitudes of the RR Lyrae stars presented in Clement's catalog and the OGLE catalog (Figure 5).

For NGC 6522 there are 17 RR Lyrae stars in the OGLE catalog (8 of Rab type and 9 of RRc type; Soszyński et al. 2014), and 10 of them are also present in the compilation given in Clement et al. (2001, edition 2017).[16] For NGC 6626 Clement's catalog presents only 10 RR Lyrae stars with mean magnitude values in the V filter (8 RRab and 2 RRc; Wehlau & Butterworth 1990). Two RR Lyrae stars toward this cluster were rejected owing to their discrepant magnitudes, being probably foreground or background field stars. A large number of 35 RR Lyrae stars (18 RRab and 17 RRc; Olech et al. 2001) are available for NGC 6362. The OGLE catalog does not provide any entry for RR Lyrae stars in the other two GCs in our sample. The mean of the mean magnitudes is also shown in Table 2 and Figure 5, as well as the standard deviation in these values.

The mean V magnitudes of the RR Lyrae stars were converted into the F625W filter, allowing a consistent comparison with the MSTO, as previously determined by us. The transformation of V magnitudes presented in Clement's and OGLE catalogs into the F625W band has been done in the following steps: conversion of the V into the R band and then from R to F625W using the Sirianni et al. (2005) ACS

[16] In Clement's catalog the RRab and RRc types are designed as RR0 and RR1, respectively, as suggested by N. N. Samus at the IAU XXVIth General Assembly, Prague 2006.

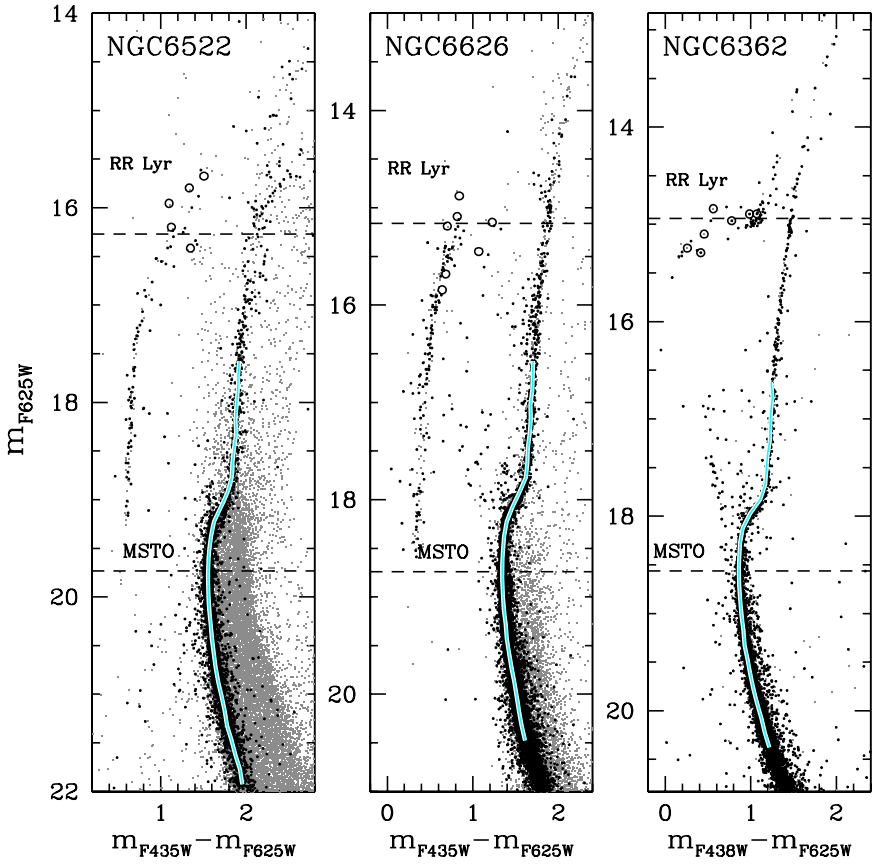

Figure 4. F625W vs. F435W–F625W CMDs of NGC 6522 and NGC 6626, and F625W vs. F438W–F625W CMD of NGC 6362. Cluster stars (black) and noncluster stars (gray) are shown in each panel. The fiducial lines (cyan solid lines) and the position of the RR Lyrae stars from Clement's catalog (open circles) that were identified in the *HST*/ACS data are also presented. The horizontal dashed lines represent the MSTO magnitude (lower line) and the average of the mean magnitudes for all RR Lyrae stars in Clement's catalog and the OGLE catalog (upper line; see Section 3.2 for details).

Table 2
Photometric Parameters from *HST* Data and RR Lyrae Stars

Cluster	MSTO F625W	RR Lyrae No. of Stars	RR Lyrae $\langle V \rangle$	RR Lyrae $\langle$F625W$\rangle$	ΔV_{TO}^{HB} $\langle$F625W$\rangle$
NGC 6522	19.73 ± 0.05	17	16.70 ± 0.05	16.27 ± 0.09	3.46 ± 0.10
NGC 6626 (M28)	18.74 ± 0.08	10	15.73 ± 0.06	15.16 ± 0.10	3.58 ± 0.13
NGC 6362	18.56 ± 0.08	35	15.26 ± 0.01	14.94 ± 0.08	3.62 ± 0.11

calibration. First, the given magnitudes have been corrected for color excess $E(V-R)$ starting with our color excess $E(B-V)$ (see Section 6) and the conversions from Fitzpatrick (1999). Subsequently we adopted the transformations from V to R using PARSEC isochrone (Bressan et al. 2012) colors.[17] The R magnitudes so derived are then converted into F625W based on Sirianni et al. (2005). As a consistency check, this transformation has also been obtained using BaSTI isochrone tables for HB stars with the same average temperature of the RR Lyrae, comparing the V magnitudes with the corresponding F625W magnitudes. This conversion requires interpolation of the data, but the results are basically identical to the previous procedure.

In a conservative approach, we can assume that the uncertainties related to the transformation from V to F625W are ∼0.08, including the ones from the reddening (∼0.04), and in the transformation from V to R (∼0.07). These uncertainties combined with those in the V filter provide the final values in Table 2.

Finally, we also calculated the magnitude difference between the MSTO and the HB as determined by the RR Lyrae stars (ΔV_{TO}^{HB}). This is a very common parameter used to constrain the ages of GCs (e.g., De Angeli et al. 2005; VandenBerg et al. 2013, and references therein) since it is distance and reddening independent. The ΔV_{TO}^{HB} parameter is particularly useful to determine relative ages when the clusters have similar metallicities and are homogeneously analyzed in terms of filters and method, as in the present case.

4. Physical Parameters from the Literature

4.1. Metallicity and Alpha-elements

Metallicities and main abundance ratios available are reported in Table 3. A spectroscopic analysis of eight RGB stars in NGC 6522 using the FLAMES-GIRAFFE spectrograph, with $R \sim 22{,}000$, was presented in Barbuy et al. (2009).

[17] Available at http://stev.oapd.inaf.it/cgi-bin/cmd.

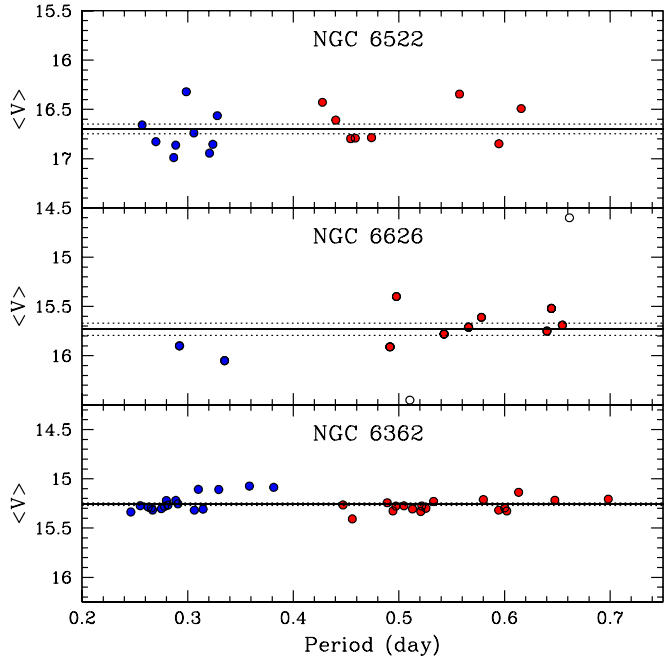

Figure 5. Mean V magnitude vs. period of the RRab (red circles) and RRc (blue circles) Lyrae stars presented in NGC 6522 (top panel), NGC 6626 (middle panel), and NGC 6362 (bottom panel). The mean of the mean V magnitudes (solid line) and its standard deviation (dotted line) are shown in each panel. Two rejected field RR Lyrae stars toward NGC 6626 (open circles) are also presented.

The authors found a metallicity of [Fe/H] $= -1.0 \pm 0.2$ together with the α-element enhancements (see Table 3). Using the same FLAMES-GIRAFFE data, Ness et al. (2014) reanalyzed the eight stars and measured [Fe/H] $= -1.15$ and a somewhat higher enhancement of α-elements. An improved analysis of four of the same RGB stars by Barbuy et al. (2014) was obtained using the FLAMES-UVES spectrograph at $R \sim 45{,}000$ and a higher signal-to-noise ratio. This resulted in [Fe/H] $= -0.95 \pm 0.15$ and α-enhancements similar to those given in Barbuy et al. (2009). Based on the DR13 release of APOGEE, J. G. Fernández-Trincado et al. (2018, in preparation) find [Fe/H] $= -1.06 \pm 0.06$ and [α/Fe] $= +0.26$ (mean of O, Mg, Si) for second-generation stars. As concerns NGC 6626, Villanova et al. (2017) recently analyzed 21 stars observed with FLAMES-UVES. They obtain [Fe/H] $= -1.29$ and abundances for 21 elements.

For NGC 6362 the spectroscopic analysis carried out by Mucciarelli et al. (2016) gives values of metallicity [Fe/H] and [Na/Fe]. Using sodium as a key indicator of stars from first and second generations (e.g., Campbell et al. 2013), Mucciarelli et al. (2016) and Villanova et al. (2017) provided two distinct [Na/Fe] values for NGC 6362 and NGC 6626, respectively. For NGC 6522 no Na excess is found in Barbuy et al. (2009, 2014), except for star B-8 in Barbuy et al. (2009). Ness et al. (2014) found three Na-normal stars and five stars with Na excess, partly due to their lower metallicities relative to Barbuy et al. (2014). Note that for NGC 6522 [α/Fe] $=$ [$\langle$(O + Mg + Si + Ca + Ti)$\rangle$/Fe], whereas for NGC 6626 [α/Fe] $=$ [$\langle$Mg + Si + Ca + Ti$\rangle$/Fe], since oxygen abundances are not derived for the latter.

The [α/Fe] values reported in Table 3 justify the adopted [α/Fe] $\sim +0.4$ available in the isochrone sets. Such α-enhancements are of the same order as measured in other clusters of the Galactic bulge (e.g., Table 4 of Bica et al. 2016).

Finally, it must be pointed out that since Mg and Si are important electron donors, they contribute to the formation of the H^- ion, which is the main opacity source at the temperatures of G–K type stars, therefore affecting the effective temperature scale of both MSTO and (mostly) RGB stellar models. The trend is that by increasing the Mg and/or Si abundance at a given [Fe/H], the RGB becomes cooler: an increase of 0.4 dex causes a decrease of about 100–150 K in $T_{\rm eff}$. Because Mg and Si (together with O and Ne) affect the difference in $T_{\rm eff}$ (and hence color) between the MSTO and the lower RGB at a fixed age, the use of such a diagnostic to determine the relative ages of star clusters having very similar [Fe/H] values will yield reliable results only if the cluster-to-cluster differences in the abundances of these elements are small, or if the effects of such differences are taken into account (see VandenBerg et al. 2012, for a detailed discussion on this issue). As a warning, we note that—as listed in Table 3—the Mg and Si abundances in these GCs might be lower than that of halo clusters.

4.2. Age, Distance, Reddening, and Structural Parameters

In Table 4 we compile literature results for the sample clusters, including ages, solar and galactocentric distances, reddening, absolute magnitudes, core radii, and concentration parameter. NGC 6522 and NGC 6626 are within the bulge volume, and NGC 6522 is located at <1 kpc from the Galactic center in Baade's Window.

As for the ages, NGC 6522 was found to be very old ($\gtrsim$13.8 Gyr) in two studies available using *HST* previous data (Meissner & Weiss 2006; Barbuy et al. 2009). For NGC 6626 there is only one relative age determination (Testa et al. 2001), suggesting that it is 1.2 ± 0.9 Gyr older than NGC 2298 (13.0 Gyr, as determined by Dotter et al. 2010). Recently, Villanova et al. (2017) argued that this cluster should be as old as M15 ($\sim$13.0 Gyr) owing to their similar BHB at the same metallicity. The inner halo cluster NGC 6362 has been studied more extensively in the literature and can be used as a reference with respect to other studies, and conversely as a comparison probe with the present clusters. Most results for this cluster indicate an age $\gtrsim$12.5 Gyr, therefore classifying it as an old GC. The only exception is the work from Meissner & Weiss (2006), where a younger age ($\sim$10 Gyr) for NGC 6362 is given, significantly younger (by $\sim$4 Gyr) than NGC 6522.

The two bulge clusters have $E(B\text{–}V) > 0.40$, while NGC 6362 has a low reddening. On the other hand, NGC 6522 and NGC 6362 present similar solar distances ($\sim$7–8 kpc), $\sim$2 kpc farther than NGC 6626.

The structural parameters indicate that NGC 6522 is a core-collapse cluster (Terndrup et al. 1998) and the most compact and least massive object ($\sim 6 \times 10^4\, M_\odot$) in our sample (Gnedin & Ostriker 1997), whereas NGC 6626 is the most massive ($\sim 4 \times 10^5\, M_\odot$) and NGC 6362 is the least compact one.

5. Isochrone Fitting

5.1. Isochrone Models

In order to compare the *HST* data for the sample clusters with theoretical models, we selected α-enhanced isochrones with canonical ($Y \sim 0.25$) and helium-enhanced ($Y = 0.30$–0.33)

Table 3
Metallicity and Chemical Abundances from High-resolution Spectroscopy

Cluster	[Fe/H]	[O/Fe]	[Mg/Fe]	[Si/Fe]	[Na/Fe]	[α/Fe]	References
NGC 6522	-1.00 ± 0.20	+0.40	+0.03	+0.23	+0.25	+0.25	B09
	-1.15 ± 0.15	⋯	+0.43(2G)	+0.42	+0.28	+0.36	N14
	-1.15 ± 0.15	⋯	−0.21(1G)	+0.42	+0.28	+0.36	N14
	-0.95 ± 0.15	+0.36	−0.07	+0.23	+0.13	+0.18	B14
	-1.06 ± 0.07	+0.33	+0.07	+0.38	⋯	+0.26	F18
NGC 6626	-1.29 ± 0.01	−0.36(2G)	+0.46(2G)	+0.34	+0.46(2G)	+0.37	V17
(M28)	-1.29 ± 0.01	+0.27(1G)	−0.04(1G)	+0.34	−0.04(1G)	+0.38	V17
NGC 6362	-1.09 ± 0.01	⋯	⋯	⋯	+0.00(1G)	⋯	M16
	-1.09 ± 0.01	⋯	⋯	⋯	+0.33(2G)	⋯	M16
	-1.07 ± 0.01	⋯	+0.54	+0.45	⋯	+0.32	M17

Note. B09—Barbuy et al. (2009); N14—Ness et al. (2014); B14—Barbuy et al. (2014); F18—J. G. Fernández-Trincado et al. (2018, in preparation); V17—Villanova et al. (2017); M16—Mucciarelli et al. (2016); M17—Massari et al. (2017).

Table 4
Age, Distances, Reddening, and Structural Parameters from Literature

Cluster	Age (Gyr)	References	$(m–M)_0$	$d_\odot$ (kpc)	R_{GC} (kpc)	$E(B-V)$	r_c (arcsec)	c ($\log(\frac{r_t}{r_c})$)	M_V	References	Mass ($\times 10^4$ $M_\odot$)	References
NGC 6522	$\gtrsim$14.0	B09	14.43	7.7	0.6	0.48	3.1	2.50c	−7.65	H96	5.93	GO97
	15.0 ± 1.1	MW06 (a)	14.34	7.4	0.8	0.66				VFO10		
	13.8 ± 1.6	MW06 (b)	14.30	7.2	<1	0.46				T98		
			14.52	7.8	0.6	0.48			−7.67	P02		
NGC 6626	14.2 ± 0.9	T01, D10	13.70	5.5	2.7	0.42	14.4	1.67	−8.16	H96	44.2	GO97
(M28)	∼13.0	V17										
NGC 6362	12.5 ± 0.25	VdB13	14.40	7.6	5.1	0.09	79.4	1.10	−6.95	H96	11.7	GO97
	12.5 ± 0.50	D10	14.55	8.1		0.07			−7.06	D10		
	13.6 ± 0.6	MF09										
	14.0	P10	14.39	7.6	5.1	0.09	72	1.17	−6.94	P10		
	$12.82^{+0.03}_{-0.04}$	WK16	14.56	8.1		0.09				WK16		
	$13.497^{+0.003}_{-0.011}$	WK17	14.44	7.7		0.10				WK17		
	10.5	MW06 (a)	14.54	8.1	5.3	0.08			−7.06	P02		
	9.0 ± 0.5	MW06 (b)										

Note. B09—Barbuy et al. (2009); D10—Dotter et al. (2010); GO97—Gnedin & Ostriker (1997); H96—Harris (1996, update in 2010); MF09—Marín-Franch et al. (2009), $1.06 \pm 0.05 \times 12.8$ Gyr (mean reference age using Dartmouth isochrones); MW06—Meissner & Weiss (2006), using their own isochrones (a) and BaSTI (b) isochrones; P10—Paust et al. (2010); P02—Piotto et al. (2002); T98—Terndrup et al. (1998); T01—Testa et al. (2001), 1.2 ± 0.90 Gyr older than NGC 2298, taken as 13.0 Gyr from D10; VFO10—Valenti et al. (2010); VdB13—VandenBerg et al. (2013); V10—Villanova et al. (2017), age comparable to M12 owing to their similar metallicity and BHB; WK16—Wagner-Kaiser et al. (2016), for two populations with $Y = 0.220$ (1G) and 0.265 (2G); WK17—Wagner-Kaiser et al. (2017), for a single population with $Y = 0.327$ and adopting [α/Fe] = +0.40.

isochrones from the Dartmouth Stellar Evolutionary Database (DSED; Dotter et al. 2008) and from BaSTI models (Pietrinferni et al. 2006).

Based on the spectroscopic results for these clusters, isochrones with [Fe/H] = −1.0, −1.15, and −1.30 and [α/Fe] = + 0.40 were employed, covering ages from 10.0 to 15.0 Gyr (in steps of 0.50 Gyr). The effects of age, metallicity, and helium enhancement in DSED and BaSTI isochrones are illustrated in Figure 6. Essentially helium-enhanced isochrones predict bluer MS and RGB, as well as fainter MSTO, than the isochrones with standard helium abundance. A $\Delta Y \sim 0.05$–0.08 can produce an effect as large as ∼0.05 in (F435W–F625W) color for the MS or RGB stars and about 0.20 mag (F625W) in the MSTO magnitude, resembling a difference of ∼0.15 dex in [Fe/H] or ∼2.5 Gyr in age. Therefore, it is expected that isochrone fits using helium-enhanced models will recover higher reddening and lower distance values, as well as younger ages. Furthermore, helium enhancement produces a remarkable change in the SGB shape, which becomes significantly steeper.

It is important to point out that the BaSTI models have been computed by neglecting the effect of atomic diffusion, which is included in the DSED models (when computing BaSTI models it was chosen not to include this effect owing to the uncertainty on the atomic diffusion coefficients). This introduces an offset in the age scale based on the two distinct model sets: the inclusion of the diffusion reduces the age by about 0.9 Gyr at the metallicity of the sample GCs (Cassisi et al. 1998, 1999, and references therein). Therefore, the BaSTI-based ages should be reduced by 0.9 Gyr, and this completely removes the apparent contradiction with the age of the universe (13.799 ± 0.021 Gyr; Planck Collaboration 2016).

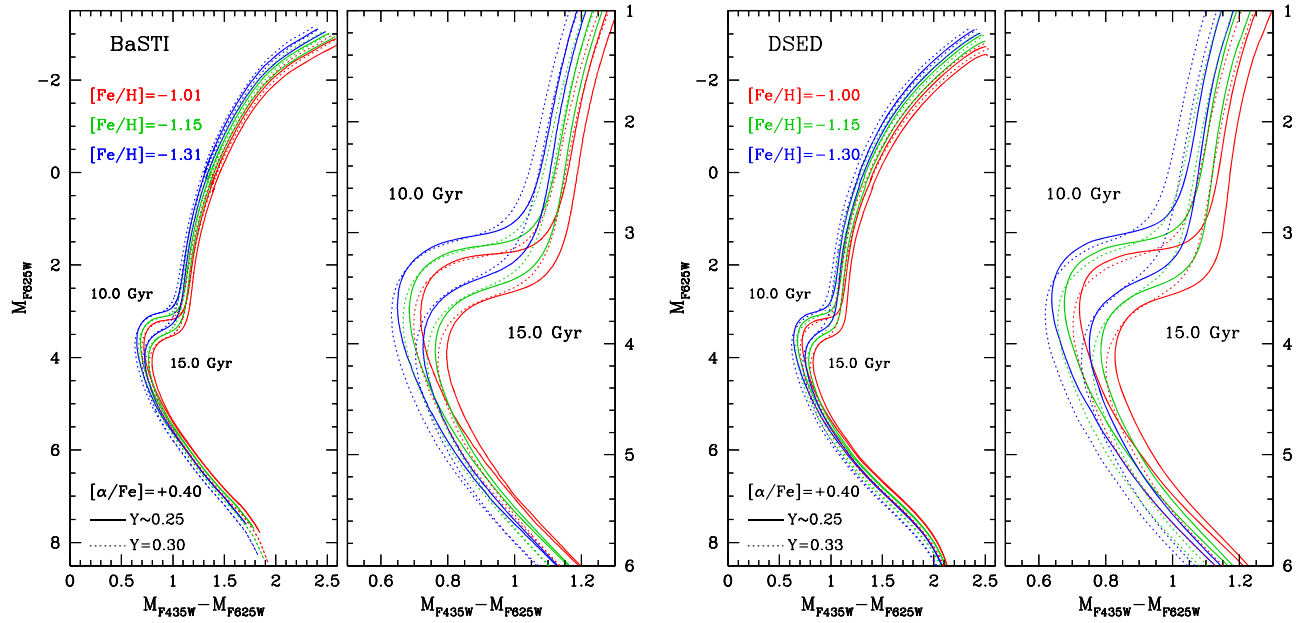

Figure 6. Isochrones from BaSTI (left panels) and Dartmouth (right panels) showing the metallicity effects for two ages (10.0 and 15.0 Gyr). All these isochrones are α-enhanced ([α/Fe] = +0.40]). Isochrones with [Fe/H] ~ -1.0 and canonical ($Y \sim 0.25$; solid lines) and enhanced ($Y = 0.30$ for BaSTI models, $Y = 0.33$ for DSED models; dotted lines) helium abundances are presented.

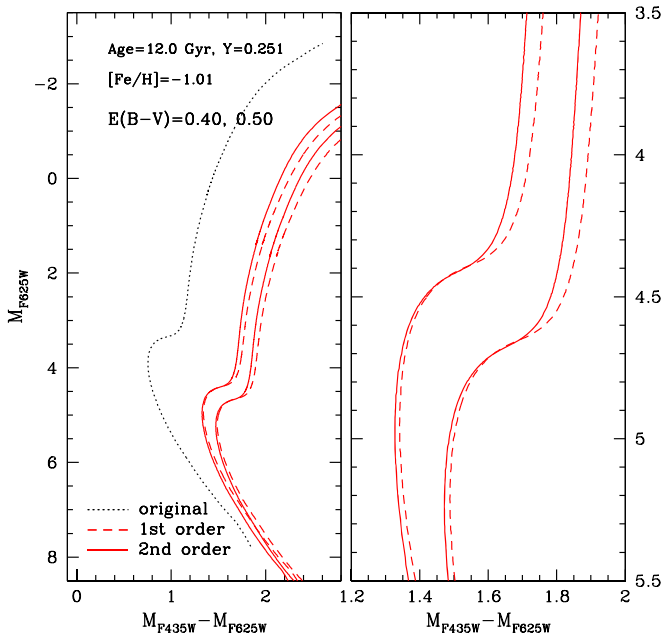

Figure 7. CMD correction for the reddening effect using a uniform $E(B-V)$ (first order; dashed lines) and a temperature-dependent one (second order; solid lines). A single α-enhanced BaSTI isochrone with 12 Gyr, $Y = 0.251$, and [Fe/H] $= -1.01$ is converted from its reddening-free position (dotted line) to the ones corresponding to the reddening values $E(B-V) = 0.40$ and 0.50.

Before using theoretical isochrones to fit the cluster CMDs, we had to consider carefully an important issue, related to the high extinction along the line of sight to some clusters in our sample, as in the case of NGC 6522 and NGC 6626, for which $A_V > 1$. It is well known that the ratio between the extinction in a given photometric band (A_λ) and A_V depends on the flux distribution of the stellar source and is in principle dependent on parameters such as the effective temperature, surface gravity, and chemical composition (see, e.g., Bedin et al. 2005; Ortolani et al. 2017, for discussions and data specific for the ACS photometric filters). As long as A_V is small, this effect is negligible and a single value of A_λ/A_V can be safely applied along the whole isochrone. But the high value of the extinction in the case of NGC 6522 and NGC 6626 makes it necessary to consider, in the fits to the observed CMD, the variation of A_λ/A_V along the isochrones due to (mainly) the change in the stellar effective temperature. In order to account for this effect when needed, we proceeded as follows: we first used the CMD 3.0 web interface,[18] which implements the results by Girardi et al. (2008), to determine the extinction in the relevant photometric filters, covering the full range of $T_{\rm eff}$ values of our isochrones and zero-age horizontal branch (ZAHB), for a suitable value of the metallicity, and for varying values of the extinction; these final extinction values in the F625W and F435W bands were then applied to the theoretical isochrones transformed to the ACS system. These $T_{\rm eff}$-dependent extinction corrections have the effect of steepening the RGB by Δ(F435W–F625W) $\sim$0.05, as shown in Figure 7; indeed, this correction is very relevant for present work, because the effect on the RGB and SGB shape is quite similar to that related to a variation in the initial He abundance.

5.2. Statistical Fiducial Line Comparisons

The age, reddening, and distance modulus of each cluster were derived from statistical comparisons between synthetic fiducial lines and the observed ones. Similar procedures have been applied to analyze *HST* CMDs of Galactic GCs (e.g., Marín-Franch et al. 2009; VandenBerg et al. 2013) and populous LMC clusters (e.g., Kerber et al. 2007). The synthetic fiducial lines were determined by the color median positions at each magnitude bin of synthetic CMDs encompassing the MS, SGB, and RGB. These CMDs were generated using DSED and BaSTI isochrones with [α/Fe] $= +0.40$, [Fe/H] $= -1.0$ (for NGC 6522, NGC 6362) and -1.15 (for NGC 6522, NGC 6362), and [Fe/H] $= -1.3$ (for NGC 6626) and different helium abundances (from $Y \sim 0.25$ to

[18] http://stev.oapd.inaf.it/cgi-bin/cmd

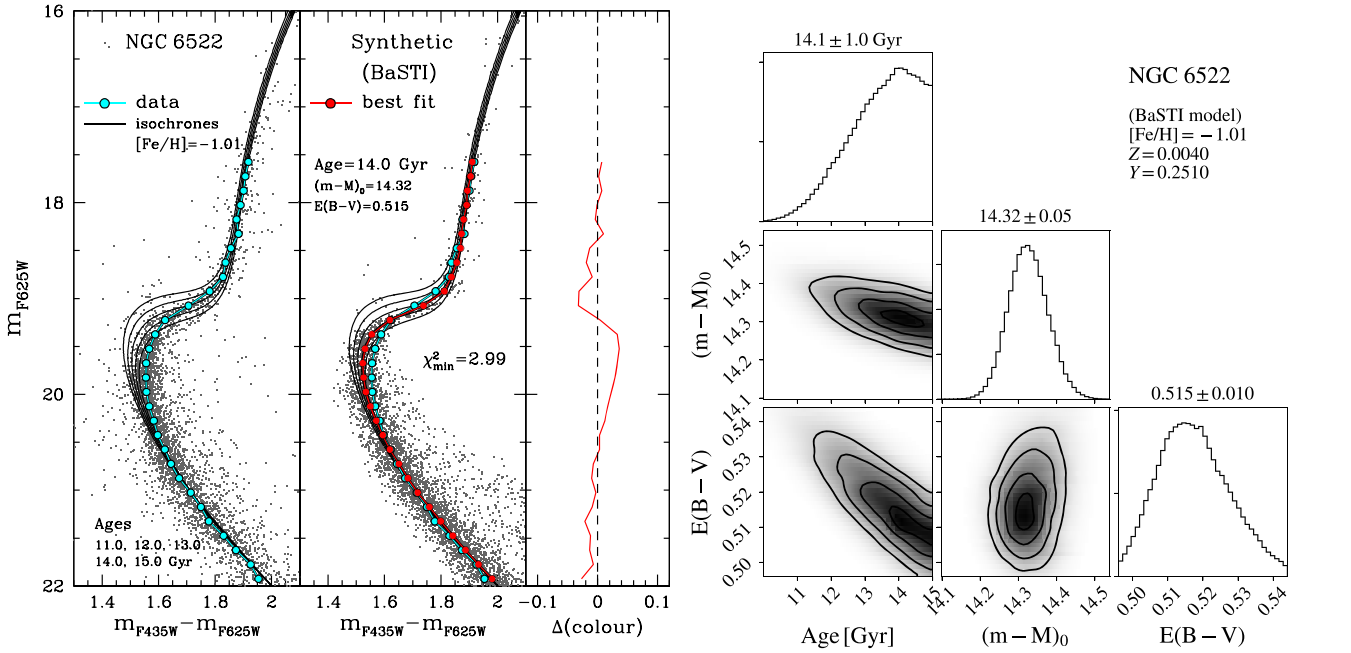

Figure 8. Left panels: observed CMD and the fiducial line for NGC 6522 compared with a synthetic CMD for the best isochrone fit using α-enhanced BaSTI models with [Fe/H] $= -1.01$ and $Y = 0.251$. Isochrones with 11.0, 12.0, 13.0, 14.0, and 15.0 Gyr are overplotted (black lines). In each panel, cluster members (left) and synthetic stars (right) are shown (gray points). The color difference between the data and the fiducial line for the best fit is also presented. Right panels: corner plots showing the output from the MCMC method. They present the one- and two-dimensional projections of the posterior probability distributions for all parameters. The contours correspond to the [0.5σ, 1σ, 1.5σ, 2σ] levels.

0.33). The synthetic CMDs explored a wide and regular model grid, typically covering Δ(age) = 5.0 Gyr, $\Delta(E(B-V)) = 0.20$, $\Delta((m\text{–}M)_0) = 0.40$, in steps of 0.50 Gyr, 0.02 mag, and 0.02 mag, respectively. Furthermore, educated guesses for photometric uncertainties (similar to the ones determined for the bulk of stars), binarity (20%), and initial mass function (Salpeter) were used in order to reproduce the observed CMD features. The χ^2 statistics was employed to compare the model (mod) and data (obs) colors, being computed for the $N_{\rm bin}$ magnitude bins along the fiducial line according to the expression

$$\chi^2 = \frac{1}{N_{\rm bin} - 1} \sum_{i=1}^{N_{\rm bin}} \left[\frac{({\rm color})_{{\rm obs},i} - ({\rm color})_{{\rm mod},i}}{\sigma_{\rm color}} \right]^2,$$

where $\sigma_{\rm color}$ is the dispersion in the median color position for the ith magnitude bin in the model (typically $\sim$0.02).

To determine the final values of the fit parameters, as well as to study the confidence intervals and correlations between them, we applied the Markov chain Monte Carlo (MCMC) sampling technique. For that purpose, we used the `emcee` code (Foreman-Mackey et al. 2013) to sample the posterior probability in the three-dimensional parameter space, assuming likelihood $\propto \exp[-\chi^2/2]$ and a uniform prior probability within the acceptable physical ranges.

Figure 8 illustrates our isochrone fitting method applied to the *HST* CMD of NGC 6522. In this fit we employed α-enhanced BaSTI models with [Fe/H] $= -1.01$ and $Y = 0.251$. The left panels in this figure present the observed CMD and its fiducial line, as well as their synthetic counterparts for the best solution, whereas the right panel shows the MCMC sampling results for NGC 6522. The complete set of results for all clusters, including all figures with the output of the MCMC, is available in the online material.

6. Results from Isochrone Fitting

6.1. NGC 6522

For this cluster two different values of metallicity were used: [Fe/H] $= -1.0$ and -1.15. The best isochrone fits using BaSTI and DSED models are shown in Figures 9 and 10. The recovered physical parameters are presented in these figures and in Table 5, including the minimum χ^2 for each set of models ($\chi^2_{\rm min}$).

The results with BaSTI isochrones indicate an age of $\sim$14.2 Gyr for this cluster, or $\sim$13.3 Gyr when corrected for the effect of atomic diffusion (See Section 5.1). On the other hand, DSED models point to $\sim$12.2 Gyr if a canonical helium abundance ($Y \sim 0.25$) is employed, or $\sim$11.4 Gyr if a $\Delta Y \sim 0.08$ is considered. The age results seem to be insensitive to the choice of metallicity and present random uncertainties that are $\sim$1.0 Gyr. In contrast, there are significant variations in distance modulus and reddening as a function of the adopted stellar evolutionary model and helium abundance. As expected, helium-enhanced models recovered solutions with shorter distances and higher reddening values, producing systematic differences of $\sim$0.13 mag in distance modulus ($\sim$0.4 kpc) and $\sim$0.04 in $E(B-V)$. Besides this, in comparison to results from BaSTI models, DSED isochrones favored isochrone fits with significantly higher values for distance and reddening.

Another remarkable result concerns the dependency of the goodness of fit with the helium abundance: as attested by the color difference between model and data and consequently by the $\chi^2_{\rm min}$ value, the shape of the observed fiducial line in the MSTO region and the SGB region seems to be better reproduced by helium-enhanced models, independently of the choice related to the stellar evolutionary model. However, in Section 7.2 we demonstrate that the helium enhancement

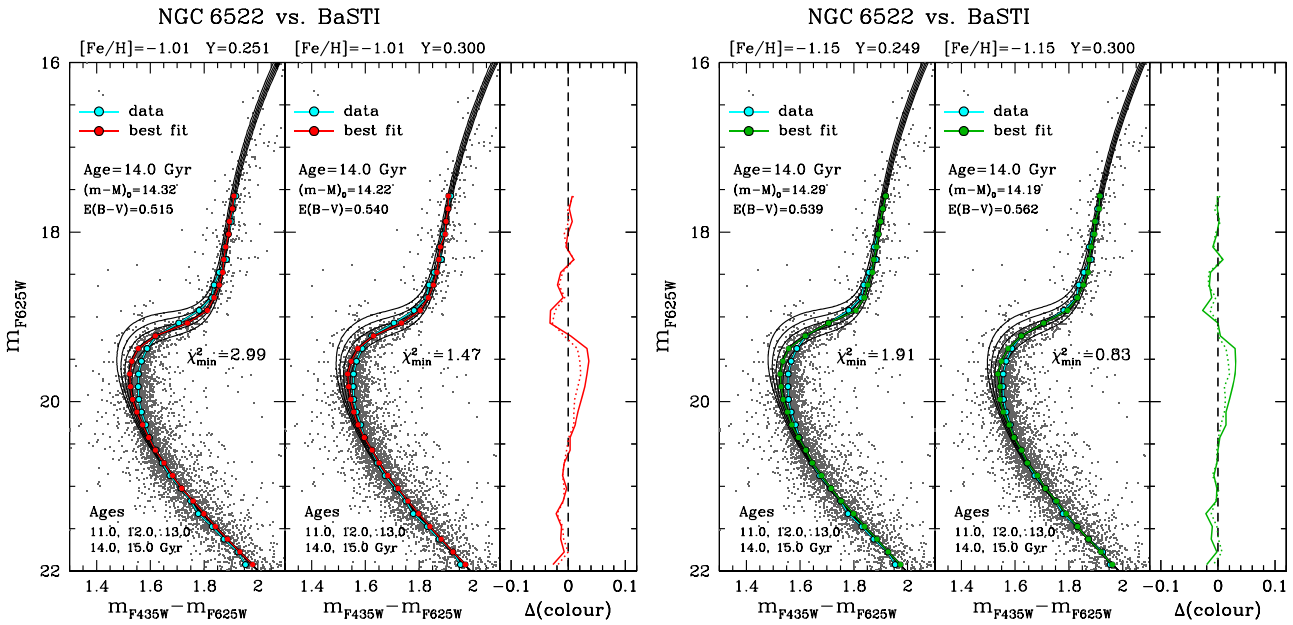

Figure 9. Left panels: observed fiducial line for NGC 6522 compared with a synthetic one for the best isochrone fit using α-enhanced BaSTI models with [Fe/H] $= -1.01$. Two different helium abundances were tested: $Y \sim 0.25$ and $Y = 0.30$. Isochrones with 11.0, 12.0, 13.0, 14.0, and 15.0 Gyr are overplotted (black lines). The cluster members are also shown (gray points). The color differences between the data and the best fiducial lines for models with $Y \sim 0.25$ (solid line) and $Y = 0.30$ (dotted line) are also presented. Right panels: same as in the left panels, but for the BaSTI models with [Fe/H] $= -1.15$.

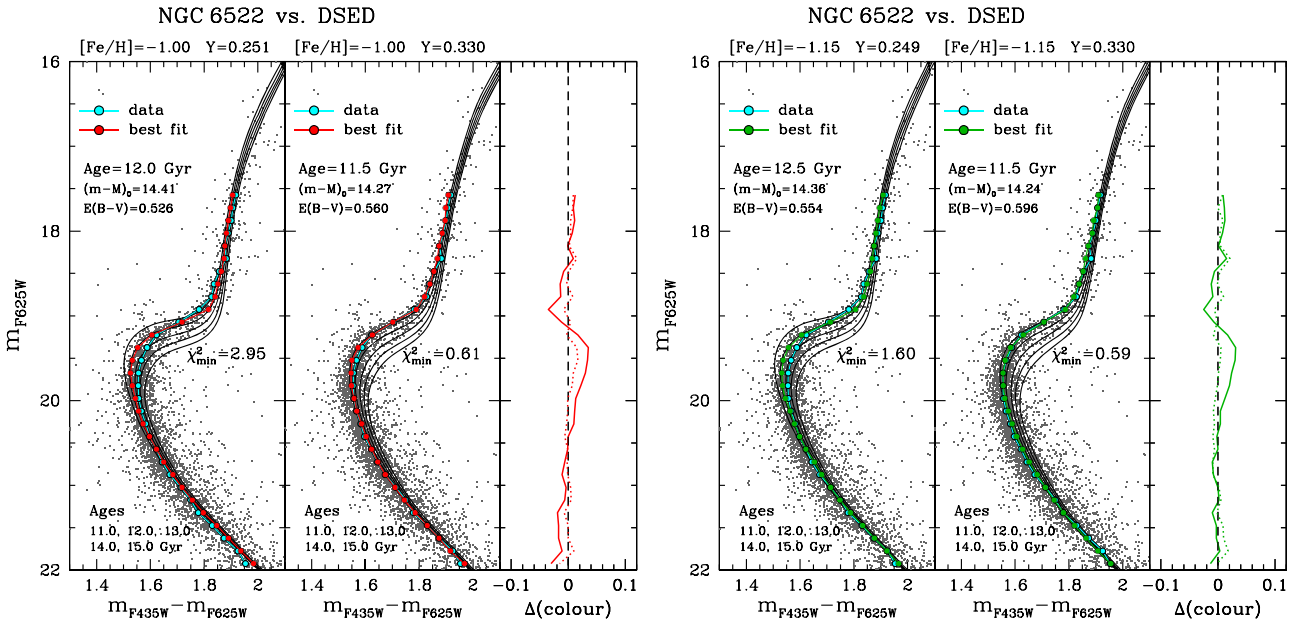

Figure 10. Same as Figure 9, but for DSED isochrones with [Fe/H] $= -1.00$ (left panels) and [Fe/H] $= -1.15$ (right panels). The DSED helium-enhanced models have $Y = 0.33$.

hypothesis is ruled out by the mean magnitude of the RR Lyrae stars.

6.2. NGC 6626

Figure 11 presents the observed fiducial line for NGC 6626 in comparison with the best isochrone fits using DSED and BaSTI stellar evolutionary models. We adopted a single metallicity for this cluster, very close to the value determined by Villanova et al. (2017). As demonstrated by the previous results related to NGC 6522, this constraint is crucial to reduce the systematic uncertainties in distance and reddening. The recovered physical parameters are shown in Table 5.

This cluster presents very similar results with respect to NGC 6522. Assuming the same helium abundance and the same stellar evolutionary model, their ages are almost identical. As occurred for NGC 6522, the goodness of fit increases significantly with the adoption of helium-enhanced models. However, as demonstrated in Section 7.2, once again a helium enhancement of $\Delta Y \sim 0.05$ is not compatible with the mean magnitude of RR Lyrae stars observed in this cluster.

6.3. NGC 6362

The eight isochrone fits for this cluster using different combinations of metallicity, helium abundance, and stellar

Table 5
Physical Parameters for NGC 6522, NGC 6626, and NGC 6362 from Isochrone Fits Using α-enhanced BaSTI and DSED Models

Cluster	Model	[Fe/H]	Z	Y	Age (Gyr)	$(m–M)_0$	$d_\odot$ (kpc)	R_{GC}	$E(B–V)$	χ^2_{min}
NGC 6522	BaSTI	−1.01	0.0040	0.2510	14.1 ± 1.0[a]	14.32 ± 0.05	7.31 ± 0.17	0.88 ± 0.12	0.515 ± 0.010	2.99
	BaSTI	−1.01	0.0037	0.3000	14.1 ± 1.0[a]	14.22 ± 0.05	6.98 ± 0.16	1.15 ± 0.14	0.540 ± 0.009	1.47
	BaSTI	−1.15	0.0029	0.2490	14.2 ± 0.9[a]	14.29 ± 0.05	7.21 ± 0.17	0.96 ± 0.13	0.539 ± 0.009	1.91
	BaSTI	−1.15	0.0027	0.3000	14.4 ± 1.0[a]	14.19 ± 0.05	6.89 ± 0.16	1.23 ± 0.14	0.562 ± 0.010	0.83
	DSED	−1.00	0.0035	0.2506	12.1 ± 1.0	14.41 ± 0.05	7.62 ± 0.18	0.67 ± 0.08	0.526 ± 0.013	2.95
	DSED	−1.00	0.0031	0.3300	11.4 ± 1.0	14.27 ± 0.05	7.14 ± 0.17	1.01 ± 0.14	0.560 ± 0.011	0.61
	DSED	−1.15	0.0023	0.2488	12.4 ± 1.0	14.36 ± 0.05	7.45 ± 0.17	0.78 ± 0.10	0.554 ± 0.011	1.60
	DSED	−1.15	0.0021	0.3300	11.4 ± 1.0	14.24 ± 0.05	7.05 ± 0.16	1.09 ± 0.13	0.596 ± 0.013	0.59
NGC 6626 (M28)	BaSTI	−1.31	0.0020	0.2480	14.3 ± 1.0[a]	13.60 ± 0.06	5.25 ± 0.15	2.96 ± 0.13	0.424 ± 0.010	1.61
	BaSTI	−1.31	0.0019	0.3000	14.0 ± 1.1[a]	13.51 ± 0.06	5.04 ± 0.14	3.15 ± 0.13	0.447 ± 0.010	0.58
	DSED	−1.30	0.0016	0.2477	12.1 ± 1.0	13.67 ± 0.06	5.42 ± 0.15	2.81 ± 0.13	0.440 ± 0.013	1.28
	DSED	−1.30	0.0015	0.3300	11.1 ± 0.9	13.57 ± 0.06	5.18 ± 0.14	3.02 ± 0.12	0.476 ± 0.011	0.39
NGC 6362	BaSTI	−1.01	0.0040	0.2510	14.3 ± 1.0[a]	14.40 ± 0.05	7.59 ± 0.17	5.11 ± 0.05	0.038 ± 0.011	1.54
	BaSTI	−1.01	0.0037	0.3000	14.3 ± 1.1[a]	14.30 ± 0.05	7.24 ± 0.17	5.04 ± 0.03	0.060 ± 0.012	1.17
	BaSTI	−1.15	0.0029	0.2490	14.7 ± 0.9[a]	14.38 ± 0.05	7.52 ± 0.17	5.02 ± 0.03	0.062 ± 0.011	1.09
	BaSTI	−1.15	0.0027	0.3000	14.8 ± 1.1[a]	14.28 ± 0.05	7.18 ± 0.17	5.02 ± 0.03	0.091 ± 0.011	1.58
	DSED	−1.00	0.0035	0.2506	12.8 ± 1.0	14.48 ± 0.05	7.87 ± 0.18	5.19 ± 0.06	0.040 ± 0.015	0.99
	DSED	−1.00	0.0031	0.3300	11.2 ± 1.2	14.36 ± 0.05	7.45 ± 0.17	5.08 ± 0.04	0.081 ± 0.016	2.09
	DSED	−1.15	0.0023	0.2488	12.8 ± 1.0	14.44 ± 0.05	7.73 ± 0.18	5.15 ± 0.05	0.070 ± 0.014	0.96
	DSED	−1.15	0.0021	0.3300	11.2 ± 1.1	14.32 ± 0.05	7.31 ± 0.17	5.05 ± 0.04	0.128 ± 0.016	2.56

Note.
[a] Ages using BaSTI models neglecting the effect of atomic diffusion. The inclusion of this effect reduces the ages by about 0.9 Gyr (See Section 5.1 for more details).

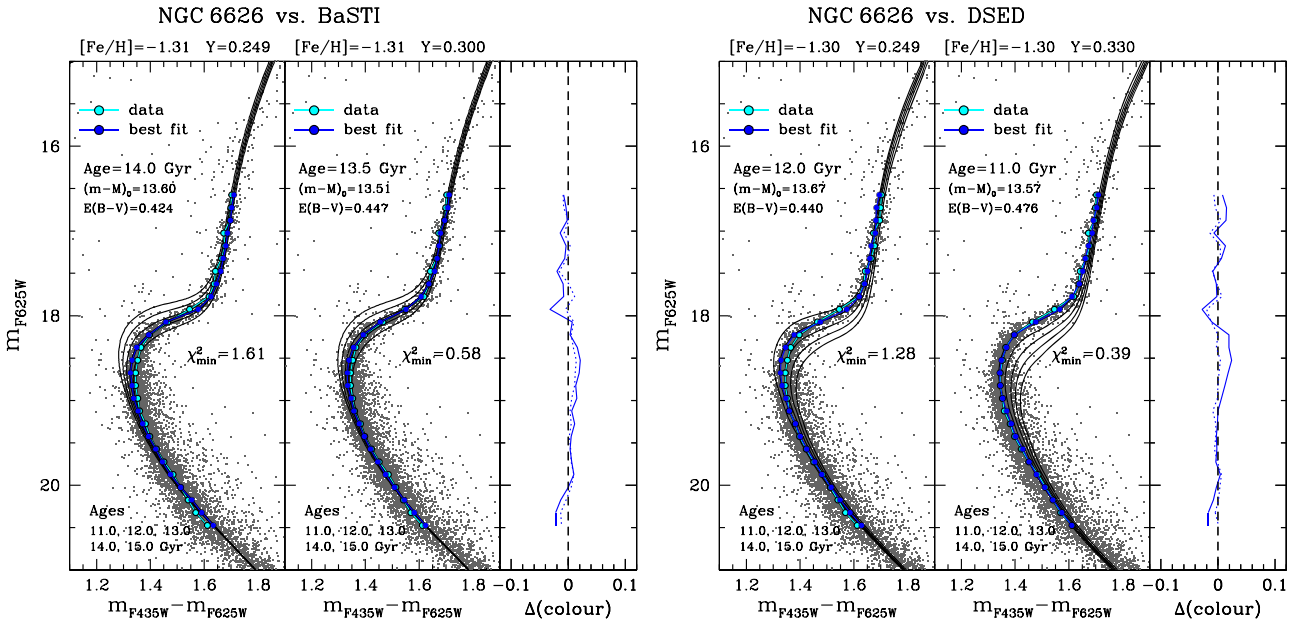

Figure 11. Same as Figure 9, but for NGC 6626 and BaSTI (left panels) and DSED (right panels) isochrones with [Fe/H] ∼ −1.3.

evolutionary models are presented in Figures 12 and 13. The physical parameters determined in this analysis are shown in Table 5.

Regardless of the choice in metallicity and in helium abundance, the BaSTI models also indicated an old age for this cluster (∼13.5 Gyr/14.5 Gyr with/without atomic diffusion). This evidence suggests a slightly older age in comparison with the other two clusters, but still in agreement if the uncertainties (∼1.0 Gyr) are taken into account. The sample clusters are found to be coeval also from the results for DSED models, within uncertainties, with ages of ∼12.4 Gyr assuming a canonical helium abundance ($Y \sim 0.25$) or ∼11.2 Gyr for $Y \sim 0.33$.

In contrast with the results for NGC 6522 and NGC 6626, Table 5 shows that the goodness of fit for NGC 6362 does not favor helium enhancement using BaSTI models, and for DSED models, a canonical helium is clearly favored. Assuming a helium abundance of $Y \sim 0.25$ and a metallicity taken as the average between the two most recent determinations ([Fe/H] = −1.08; Mucciarelli et al. 2016; Massari et al. 2017), we get an

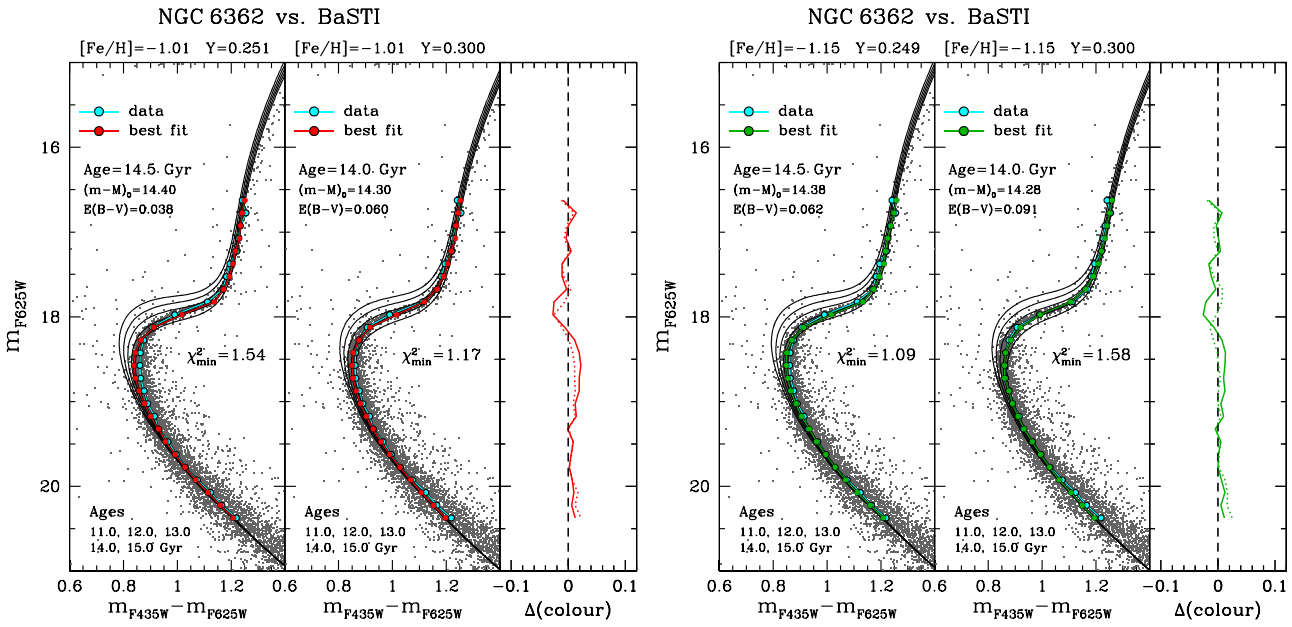

Figure 12. Same as Figure 9, but for NGC 6362.

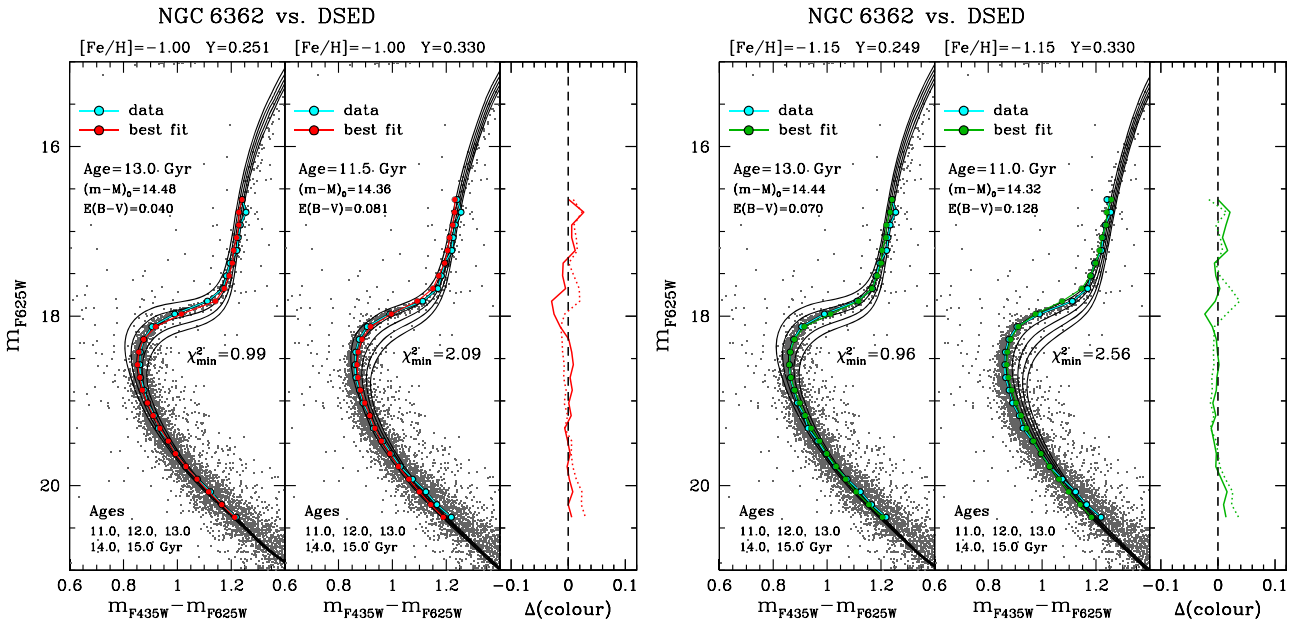

Figure 13. Same as Figure 10, but for NGC 6362.

intrinsic distance modulus of 14.39 (BaSTI) or 14.46 (DSED) and $E(B-V)$ of 0.050 (BaSTI) or 0.055 (DSED).

7. Discussion

Figure 14 summarizes the best isochrone fits to the MSTO, SGB, and RGB from the statistical analysis, together with the newly calculated tracks for the ZAHB, with all models from BaSTI. For NGC 6626 and NGC 6362 the fits are remarkably good all along the sequences. For NGC 6522 the SGB-RGB sequences are well fitted, although there is a slight offset around the MSTO. The theoretical ZAHB location is bluer/brighter than the observed distribution. We postpone a detailed investigation of this issue to a forthcoming paper; however, we note that a variation (increase) of the adopted metallicity (see data in Table 3) would help in improving the quality of the fit. If a higher helium is adopted (e.g., $Y = 0.30$), the HB models have a higher luminosity by ∼0.25 mag, at the color of the RR Lyrae.

7.1. Comparisons with Literature

From a comparison between the present results and literature results (Table 4), we confirm an age $\gtrsim$12.0 Gyr for all clusters under the assumption of a canonical helium abundance. A very old age of ∼14.0 Gyr (or 13 Gyr if corrected for diffusion) for NGC 6522 and NGC 6626 obtained by the preceding studies using *HST* data (Testa et al. 2001; Meissner & Weiss 2006; Barbuy et al. 2009) is in good agreement with our results using BaSTI models. Note that Testa et al. (2001) found evidence for a canonical helium abundance in NGC 6626.

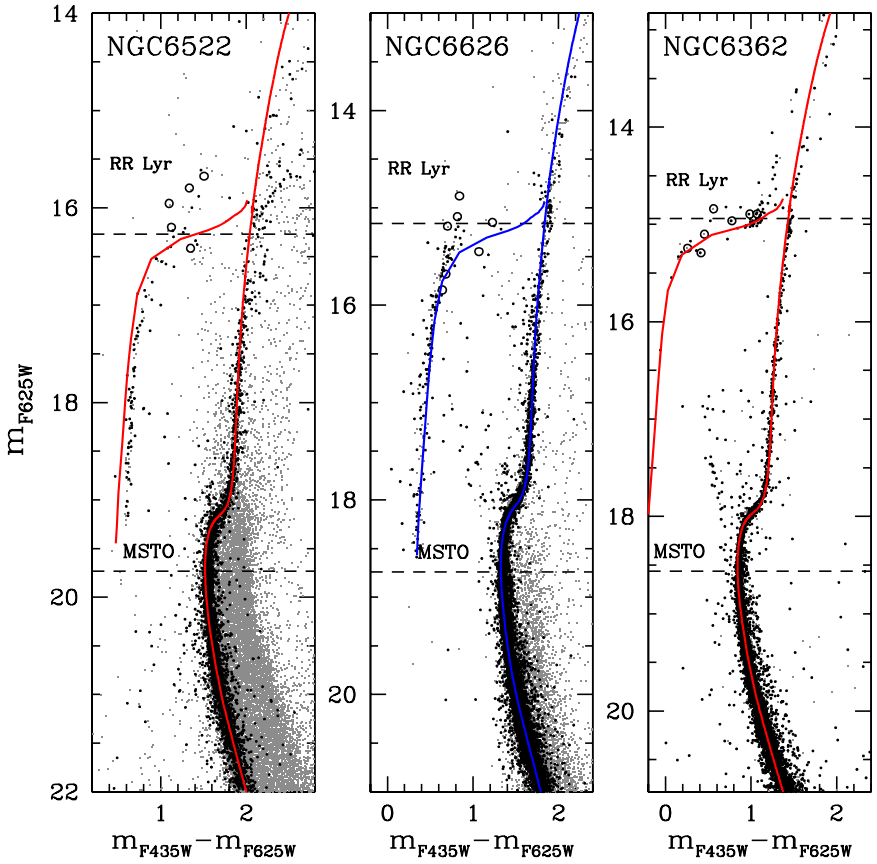

Figure 14. F626W vs. F435W–F625W CMDs for the three sample clusters. BaSTI isochrones of 14 Gyr, $Y = 0.25$ are shown as red sequences corresponding to [Fe/H] $= -1.01$ and blue ones corresponding to [Fe/H] $= -1.31$. The blue ZAHB sequence corresponds to tracks with ($Z = 0.003$, $Y = 0.251$), and the red ZAHB sequence corresponds to ($Z = 0.004$, $Y = 0.251$). Dashed lines represent the MSTO and HB levels (as in Figure 4).

The ages obtained for NGC 6362 using BaSTI models (∼14.0 Gyr) are compatible with the ones from Marín-Franch et al. (2009) and Paust et al. (2010), whereas the ages ∼13.0 Gyr from our fits using DSED models, and BaSTI models if diffusion is taken into account, in both cases with a canonical helium abundance, are in better agreement with results from Dotter et al. (2010), VandenBerg et al. (2013), and Wagner-Kaiser et al. (2016). The distances and reddening values presented in our paper and those in the literature are comparable, but our results favor slightly shorter solar and galactocentric distances and slightly lower $E(B-V)$ values.

Ages of ∼12.5 Gyr are indicated by our fits with DSED isochrones for the three clusters and derivations for other clusters using the same set of isochrones in the literature. Our results also pointed out that these clusters are located at shorter solar distances and have lower reddening values than previously thought.

Concerning NGC 6522 structural parameters, we found a core radius of 12.32 ± 0.26 arcsec, approximately four times higher than the one from Trager et al. (1995) (3.1 arcsec), who classified this cluster as core collapse. Due to the high stellar contamination and high reddening toward this cluster, the analysis performed by Trager et al. (1995) over surface brightness profiles obtained from ground-based photometry likely underestimated the core radius for NGC 6522. Assuming the average solar distances recovered by us for NGC 6522 (7.2 kpc), NGC 6626 (5.2 kpc), and NGC 6362 (7.5 kpc), their intrinsic core radii are 0.43, 0.32, and 3.3 pc, respectively. This reveals that NGC 6626 is in fact the most compact cluster in our sample.

7.2. Constraints from RR Lyrae Stars

The RR Lyrae stars provide independent constraints on the apparent distance modulus, helium abundance, and age. First, to bypass the theoretical limitations from the stellar evolutionary models and to avoid using a conversion from V to F625W, we analyzed the V magnitude of the RR Lyrae stars directly from Clement's catalog and the OGLE catalog, comparing them with two empirical average $\langle M_V \rangle$ determinations for the RR Lyrae. For this purpose we used the very recent M_V–[Fe/H] calibrated relations for RR Lyrae stars from the Gaia Collaboration (2017) based on Tycho-*Gaia* Astrometric Solution (TGAS). Since they employed three different methods to perform such calibration, we assumed the mean M_V solution for these approaches, taking into account three distinct sources of uncertainties: (1) ∼0.10 dex in [Fe/H] (0.02 mag); (2) the stochastic effects in the fits (0.04 mag); (3) and the main one, the systematics due to the different solutions (0.10). Assuming [Fe/H] $= -1.07 \pm 0.10$ as the metallicity of NGC 6522 and NGC 6362, we obtained $\langle M_V \rangle = 0.67 \pm 0.11$ for their RR Lyrae stars. Since NGC 6626 is slightly more metal-poor ([Fe/H] $= -1.30 \pm 0.10$), such variable stars should be slightly brighter ($\langle M_V \rangle = 0.62 \pm 0.11$) in this cluster. Due to the similarity with the metallicity of the RR Lyrae star itself ([Fe/H] $= -1.16$), these values are very close

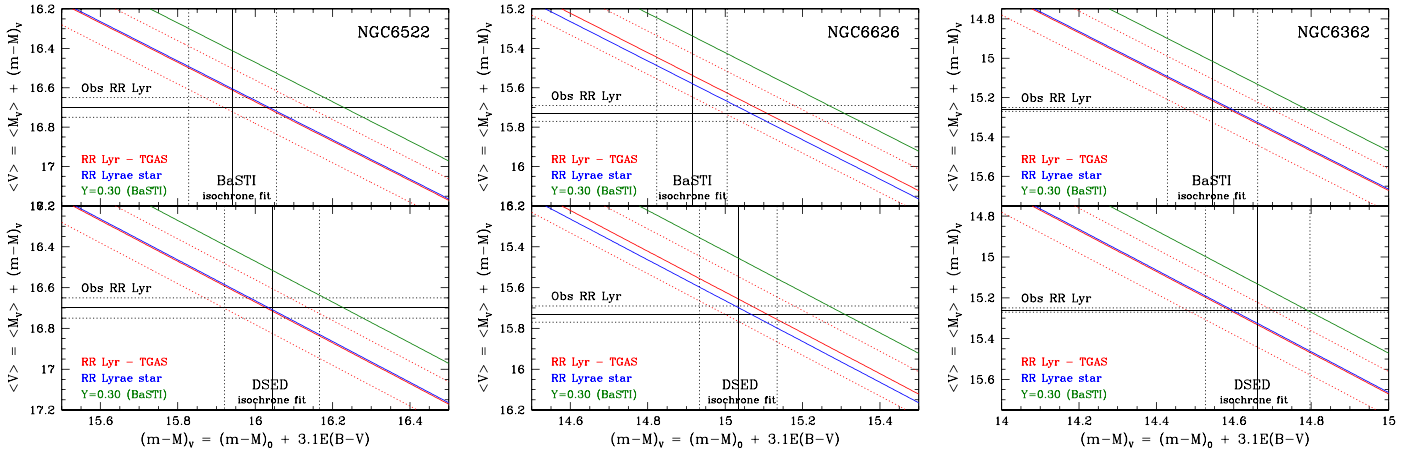

Figure 15. Predicted average V magnitude for the RR Lyrae stars as a function of the apparent distance modulus in V for NGC 6522 (left panels), NGC 6626 (middle panels), and NGC 6362 (right panels). The analysis is done over two empirical $\langle M_V \rangle$ RR Lyrae values: the recent one obtained by the Gaia Collaboration (2017; red solid lines, with 1σ confidence level marked by red dotted lines), and the one for the RR Lyrae star itself (blue solid line; Catelan & Cortés 2008). The results for the apparent distance modulus in V from the isochrone fits using BaSTI (top panels) and DSED (bottom panels) are presented (vertical solid lines) within the 1σ confidence level (dotted lines). The average of the mean RR Lyrae V magnitudes and its standard deviation are depicted in each panel (horizontal solid and dotted lines, respectively). The expected increment of -0.20 mag in V predicted by the BaSTI models due to a helium enhancement of $\Delta Y \sim 0.05$ in the canonical helium abundance for a cluster with [Fe/H] ~ -1.15 ($Y \sim 0.25$) is also shown (green solid lines).

to the one found for the prototype of this class of variable stars ($\langle M_V \rangle = 0.66 \pm 0.14$; Catelan & Cortés 2008).

Figure 15 presents the expected apparent V magnitude for the RR Lyrae stars as a function of the apparent distance modulus in V ($(m\text{–}M)_0 + A_V$) for all clusters analyzed in this work. It is clear from these plots that the apparent distance moduli from the isochrone fits agree within 1σ with what would be expected to bring the absolute magnitudes for the RR Lyrae stars to the observed ones. The only possible exception is the solution for NGC 6626 using BaSTI models, where a higher apparent distance modulus seems to be required.

We also checked whether the isochrone fits and the observed RR Lyrae stars can be consistent with helium-enhanced stars. BaSTI models predict that RR Lyrae stars with $Y = 0.30$ should be ∼0.20 mag brighter in V than ones with a canonical helium abundance for a metallicity of [Fe/H] ~ -1.15 ($Y \sim 0.25$). The results for this simple experiment are also depicted in Figure 15, clearly revealing that such bright magnitudes are not compatible with the mean V magnitude of the RR Lyrae stars observed in these clusters at the expected apparent distance moduli, therefore rejecting a helium enhancement of $\Delta Y \sim 0.05$. In fact, the recent analysis of the red giant branch bump performed by Lagioia et al. (2018) on the data from the *HST* UV Legacy Survey of Galactic GCs supports the hypothesis that the variations in the average helium abundance between distinct subpopulations are lower than $\Delta Y \lesssim 0.03$.

Taking the advantage that all clusters have similar metallicities and their MSTO and RR Lyrae mean magnitudes were homogeneously derived in the same filter, we computed the $\Delta V_{\rm TO}^{\rm HB}$ parameter in F625W to check whether there is any indication of age differences between these clusters. The results presented in Table 2 reveal similar $\Delta V_{\rm TO}^{\rm HB}$ values within the uncertainties; therefore, these clusters are probably coeval within ∼1.0 Gyr. Further investigations to discover new RR Lyrae stars in the cores of NGC 6522 and NGC 6626, as well as accurate MSTO determinations in the V filter, can reduce the uncertainties in $\Delta V_{\rm TO}^{\rm HB}$ and reveal some age difference.

7.3. Testing the Presence of Multiple Stellar Populations

The high quality of *HST* data and proper-motion-cleaned CMDs allows us to investigate the presence of multiple stellar populations (MPs) in NGC 6522. This is the first time that this kind of analysis is employed in this cluster.

The presence of more than one stellar population in NGC 6362 was also detected by combining optical *HST* and UV ground-based photometry. Dalessandro et al. (2014) have demonstrated that the RGB of NGC 6362 is split into two separate sequences. A deep photometric analysis performed by Piotto et al. (2015) and Milone et al. (2017) using UV–optical *HST* data clearly revealed the presence of these two stellar populations even for the MS stars. These results were recently corroborated by the high-resolution spectroscopic analysis performed by Mucciarelli et al. (2016) and Massari et al. (2017).

Concerning NGC 6626, the signature of MPs was revealed by the abundance analysis of 17 RGB stars from Villanova et al. (2017), which presented an Na–O anticorrelation and an Na–Al correlation. No photometric evidence of MPs in this cluster was found so far.

In order to detect a possible signature of MPs, we analyzed the SGB morphology. In the left panel of Figure 16 it is shown that, in the $m_{\rm F625W}$ versus $m_{\rm F435W}-m_{\rm F625W}$ proper-motion-cleaned CMD, the SGB of NGC 6522 is formed by two components: a more populated bright and blue SGB (potentially associated with a second stellar generation—2G) and a less populated faint and red SGB (a first stellar generation—1G).

An analysis of the ratio between the number of stars in each SGB population and the total number of SGB stars is performed. The left panels of Figure 16 show the procedure adopted. First, the SGB sequence is rectified using the procedure described in detail in Milone et al. (2009) and Bellini et al. (2013). The result is shown in the bottom right panel of Figure 16. The top right panel shows the abscissa distribution (the bin size of the histogram is equal to 0.15). Stars with 0.05 mag from the median of this distribution are the candidates to a 1G population (red points). By counting stars

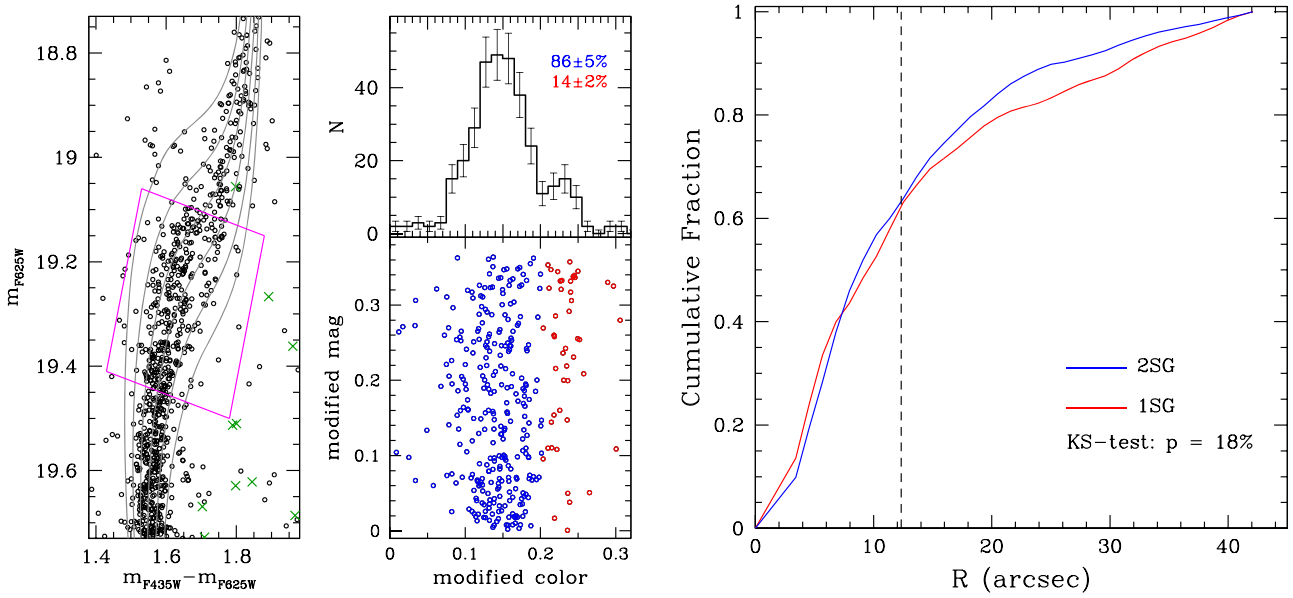

Figure 16. Left panels: SGB of NGC 6522 zoomed in, and ratio of candidates of first (red) to second (blue) stellar generations. DSED α-enhanced isochrones for [Fe/H] $= -1.01$ and $Y = 0.25$ with 10.0, 11.0, 12.0, 13.0, 14.0, and 15.0 Gyr are overplotted. The expected residual field stars are also presented (green crosses). Right panel: radial cumulative fraction distribution. The core radius (dashed line) and the K-S probability are also given.

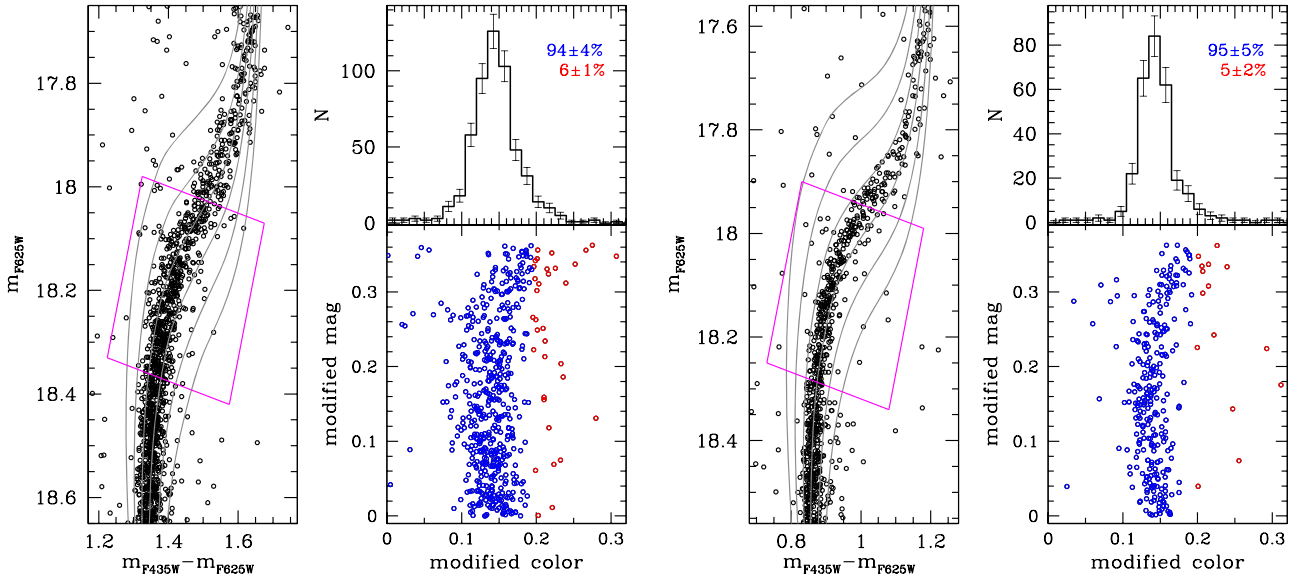

Figure 17. Same as the left panels of Figure 16, but for NGC 6626 (left panels) and NGC 6362 (right panels).

before and after this threshold, the fraction of 1G and 2G stars was determined. The results indicate that 14% ± 2% and 86% ± 5% of the stars belong to the 1G and 2G, respectively. Poisson uncertainties were assumed.

The right panel of Figure 16 presents the radial cumulative fraction distribution of the 1G and 2G stars. The two distributions seem to agree inside the core radius; however, at larger radii the 2G stars are more concentrated than the 1G stars. A Kolmogorov–Smirnov (K-S) test provides a probability of 18% that the two samples were drawn from the same underlying distribution.

To check whether the 1G sample is related to residual contaminating field stars, we compute the expected number of such stars in the proper-motion-cleaned CMD taking into account the spatial and kinematical information. First, we defined a distance from the cluster center where the field stars are dominant ($R > R_{\rm field} = 100$ arcsec). After that, we selected those with proper motions larger than 0.50 pixels (see Figure 2). Taking into account the areas in the sky and in the VPD that are covered by the cluster and field stars, we found 110 stars that might be contaminating the cluster sample. As can be seen in Figure 16, these stars are outside the box used to analyze the presence of multiple populations, so they cannot explain the wide SGB observed in this cluster.

In order to do a comparative study, we proceed with the same analysis for the two other clusters. These results are presented in Figure 17. As can be seen in both panels, no more than 6% ± 2% of the stars in NGC 6626 and NGC 6362 could be associated with a 1G by the same method. This result suggests that the 1G fraction of 14% ± 2% for NGC 6522 is a meaningful result, as well as that the 1G proportion is probably a minimum value, and that a higher proportion might be

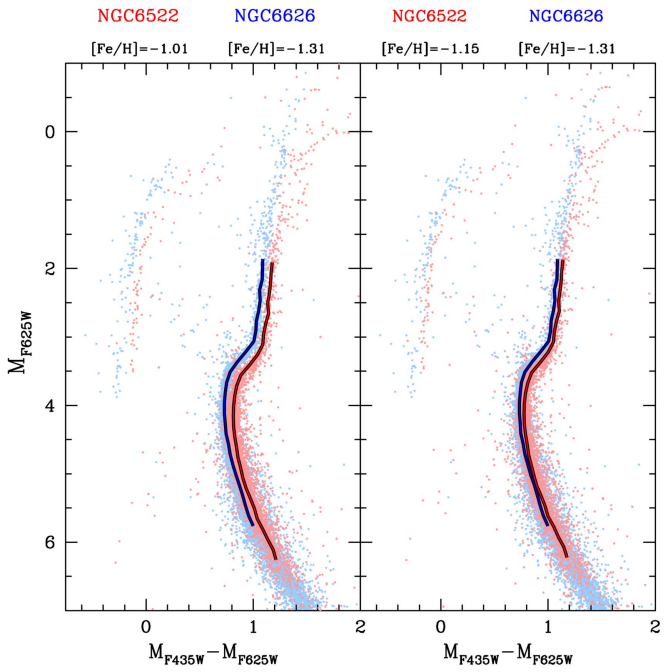

Figure 18. CMDs and fiducial lines of NGC 6522 and NGC 6626 in absolute magnitudes M_{F625W} vs. $M_{F435W}-M_{F625W}$. The conversion from observed magnitudes to the absolute ones takes into account the BaSTI stellar evolutionary models for the metallicities informed in each panel, as well as the distance moduli and reddening values that are consistent with the isochrone fits. A canonical helium abundance of $Y \sim 0.25$ was assumed.

revealed when UV colors will be available. This is expected because for NGC 6362 we find a low 1G fraction, whereas Milone et al. (2017) and Wagner-Kaiser et al. (2016), analyzing UV–optical *HST* data, determined higher values of 57.4% ± 3.5% and $38.5^{+2.6}_{-2.5}$%, respectively.

7.4. Final Remarks

The combined constraints from MSTO-SGB-RGB and HB allowed us to conclude on final values of age, helium abundance, distance, and reddening for the sample clusters. While the statistical comparisons of observed fiducial lines and theoretical ones (Figure 9) appear to lead to the possibility of higher-than-primordial helium abundances, the HB and RR Lyrae levels, compared with theoretical models, imposed a normal helium content.

The observed CMDs of NGC 6522 and NGC 6626 are very similar (despite their differences in distance and reddening); therefore, in the absolute magnitudes and colors they should almost coincide. To verify this, in Figure 18 we show the CMDs and fiducial lines of NGC 6522 and NGC 6626 transformed to absolute magnitudes and colors. Since the retrieved distance modulus and reddening do depend on the adopted metallicity, in the left and right panels of Figure 18 we present the comparison between the two clusters by adopting the parameters derived when assuming [Fe/H] = −1.0 and [Fe/H] = −1.15 for NGC 6522, respectively. The reddening and distance modulus corrections change with metallicity and lead the HB to fit better the sequences of NGC 6626 in the latter. With regard to the metallicity and abundances from high-resolution spectroscopy of NGC 6522, we should note two main issues: (a) [α/Fe] < +0.4 (Table 3), and in particular, recalling that the bulk of stars are of a 2G generation, oxygen should be lower, whereas the models assume [α/Fe] = +0.4; (b) Na is enhanced, since the bulk of stars belong to a second generation. These abundance variations can explain the need for a change in metallicity, with respect to NGC 6626. This shows the need, in the future, to have models taking into account a range of element abundances, in particular O, Na, Al, Mg, and overall alpha-elements (Si, Ca, Ti, besides O, Mg).

8. Conclusions

We analyzed *HST* proper-motion-cleaned CMDs of the bulge GCs NGC 6522 and NGC 6626, together with the inner halo cluster NGC 6362, for comparison purposes. The three clusters have similar metallicities ($-1.3 \lesssim$ [Fe/H] $\lesssim -1.0$) and alpha-enhancements ([α/Fe] $\sim +0.4$). They were observed in the same filters and (in the case of NGC 6522 and NGC 6626) in two epochs, making it possible to select the likely cluster members. Thus, these homogeneous and high-photometric-precision data allowed a detailed comparative analysis.

In this study we addressed the fundamental problem of deriving age, reddening, and distance consistently, based on statistical isochrone fitting and RR Lyrae analysis, including variable helium content. The isochrone sets BaSTI and DSED were used, chosen because they offer the needed parameters, in particular with regard to helium and alpha-element abundances.

The use of BaSTI models leads to coeval ages of ∼13.0 Gyr for the three clusters, or ∼14.0 Gyr if the atomic diffusion is neglected, independently of the helium content. The results from DSED isochrones with canonical helium abundances point to an age of ∼12.5 ± 0.5 Gyr for the clusters, in very good agreement with ages given by Dotter et al. (2010), VandenBerg et al. (2013), and Wagner-Kaiser et al. (2016) for NGC 6362. The fact that NGC 6522 and NGC 6626 have almost identical HB morphology, as shown in Figure 18, while at the same their metallicities differ by ∼0.2–0.3 dex from high-resolution spectroscopic studies, indicates that NGC 6522 should be older than NGC 6626.

The shape of the observed fiducial lines indicates some evidence of helium enhancement for NGC 6522 and NGC 6626, but the average V magnitudes of RR Lyrae stars from Clement's catalog and the OGLE catalog tend to rule out this hypothesis, since there is a good agreement between these values and those expected from the recent empirical calibration for the $\langle M_V \rangle$ Galactic RR Lyrae stars performed by the Gaia Collaboration (2017) (assuming the apparent distance moduli from our isochrone fits). If the observed RR Lyrae stars in these clusters were helium enhanced by $\Delta Y \sim 0.05$, they should be about 0.20 mag brighter on average, as predicted by BaSTI models. Further inspection of HB morphology and new stellar evolutionary models will be the subject of a future work.

For the first time based on CMDs, we revealed that NGC 6522 has at least two stellar populations, in proportions of approximately 86% (2G) and 14% (1G). According to the study by Milone et al. (2017), in his classification of type II GCs, the clusters that show clearly two stellar populations in their so-called chromosome maps show a split subgiant branch (SGB) also in optical colors. NGC 6522 does show a split in the SGB in optical colors, whereas UV colors are not available for this cluster for a definitive diagnostic as type II. The type I clusters show a split SGB only in UV colors. This is the case of NGC 6362, where a double stellar population is clearly detected with the UV colors, as shown by Piotto et al. (2015) and Milone et al. (2017). For NGC 6626, with the available

optical data, there is no evidence so far of multiple stellar populations.

Under the assumption that the total mass of NGC 6522 is around half of that of NGC 6362 (Gnedin & Ostriker 1997), NGC 6522 establishes a new lower GC mass limit where both photometric and spectroscopic signatures of multiple populations are present.

As a summary of main results, we emphasize that some parameters not available in the literature for these clusters were derived in the present work, in particular the age of NGC 6626, more precise ages for NGC 6522, and the multiple stellar populations of NGC 6522.

We conclude that the sample clusters, characterized by a moderate metallicity of [Fe/H] ~ -1.0 and enhanced α-to-iron ratios, are among the oldest objects in the Galaxy. This confirms that objects of this metallicity could have been formed from material previously enriched as proposed in well-accepted scenarios of bulge formation with fast chemical enrichment (Matteucci & Brocato 1990; Cescutti et al. 2008; Friaça & Barbuy 2017). It would be of great interest to have additional high-resolution spectroscopy of stars in these clusters and to have NGC 6522 observed in UV filters to further probe its multiple stellar populations.

L.K., B.B., and E.B. acknowledge partial financial support from FAPESP, CNPq, and CAPES. D.N. and S.O. acknowledge support by the Università degli Studi di Padova Progetto di Ateneo CPDA141214, "Toward Understanding Complex Star Formation in Galactic GCs." S.C. acknowledges the financial support by PRIN-INAF2014 (PI: S. Cassisi) and the Economy and Competitiveness Ministry of the Kingdom of Spain (grant AYA2013-42781-P). M.L. recognizes partial support by PRIN-INAF2014, "The Kaleidoscope of Stellar Populations in Galactic Globular Clusters with Hubble Space Telescope." R.G.V. acknowledges the support from FAPESP (grant 2012/20364-4).

Facility: HST(ACS, WFPC2).

ORCID iDs

L. O. Kerber https://orcid.org/0000-0002-7435-8748
D. Nardiello https://orcid.org/0000-0003-1149-3659
S. Cassisi https://orcid.org/0000-0001-5870-3735

References

Anderson, J., Bedin, L. R., Piotto, G., Yadav, R. S., & Bellini, A. 2006, A&A, 454, 1029
Anderson, J., & King, I. R. 2006, Instrument Science Report ACS 2006-01, 34
Anderson, J., Sarajedini, A., Bedin, L. R., et al. 2008, AJ, 135, 2055
Barbuy, B., Chiappini, C., Cantelli, E., et al. 2014, A&A, 570, A76
Barbuy, B., Zoccali, M., Ortolani, S., et al. 2009, A&A, 507, 405
Bedin, L. R., Cassisi, S., Castelli, F., et al. 2005, MNRAS, 357, 1038
Bedin, L. R., Piotto, G., & Anderson, J. 2009, A&A, 497, 755
Bellini, A., Bedin, L. R., Piotto, G., et al. 2010, A&A, 513, A50
Bellini, A., Piotto, G., Milone, A., et al. 2013, ApJ, 765, 32
Bica, E., Ortolani, S., & Barbuy, B. 2016, PASA, 33, 28
Bressan, A., Marigo, P., Girardi, L., et al. 2012, MNRAS, 427, 127
Campbell, S. W., D'Orazi, V., Yong, D., et al. 2013, Natur, 498, 198
Cassisi, S., Castellani, V., degl'Innocenti, S., Salaris, M., & Weiss, A. 1999, A&AS, 134, 103
Cassisi, S., Castellani, V., degl'Innocenti, S., & Weiss, A. 1998, A&AS, 129, 267
Catelan, M., & Cortés 2008, ApJL, 676, L135
Cescutti, G., Matteucci, F., & Lanfranchi, G. 2008, A&A, 491, 401
Clement, C. M., Muzzin, A., Dufton, Q., et al. 2001, AJ, 122, 2587
Dalessandro, E., Massari, D., Bellazzini, M., et al. 2014, ApJL, 791, L4
De Angeli, F., Piotto, G., Cassisi, S., et al. 2005, AJ, 130, 116
Dotter, A., Chaboyer, B., Jevremović, D., et al. 2008, ApJS, 178, 89
Dotter, A., Sarajedini, A., Anderson, J., et al. 2010, ApJ, 708, 698
Ferraro, F. R., Dalessandro, E., Mucciarelli, A., et al. 2009, Natur, 462, 483
Ferraro, F. R., Massari, D., Dalessandro, E., et al. 2016, ApJ, 828, 75
Fitzpatrick, E. L. 1999, PASP, 111, 63
Foreman-Mackey, D., Hogg, D. W., Lang, D., & Goodman, J. 2013, PASP, 125, 306
Friaça, A. C. S., & Barbuy, B. 2017, A&A, 598, 121
Gaia Collaboration 2017, A&A, 605, A79
Girardi, L., Dalcanton, J., Williams, B., et al. 2008, PASP, 120, 583
Gnedin, O. Y., & Ostriker, J. P. 1997, ApJ, 474, 223
Harris, W. E. 1996, AJ, 112, 1487
Kerber, L., Santiago, B., & Brocato, E. 2007, A&A, 462, 139
King, I. 1962, AJ, 67, 471
Lagioia, E. P., Milone, A. P., Marino, A. F., et al. 2018, MNRAS, in press
Lee, Y.-W., Demarque, P., & Zinn, R. 1994, ApJ, 423, 248
Libralato, M., Bellini, A., Bedin, L. R., et al. 2014, A&A, 563, 80
Majewski, S. R., APOGEE Team & APOGEE-2 Team 2016, AN, 337, 863
Marín-Franch, A., Aparicio, A., Piotto, G., et al. 2009, ApJ, 694, 1498
Massari, D., Mucciarelli, A., Dalessandro, E., et al. 2017, MNRAS, 468, 1249
Matteucci, F., & Brocato, E. 1990, ApJ, 365, 539
Meissner, F., & Weiss, A. 2006, A&A, 456, 1085
Milone, A. P., Marino, A. F., Piotto, G., et al. 2015, ApJ, 808, 51
Milone, A. P., Piotto, G., Bedin, L. R., et al. 2012, A&A, 540, A16
Milone, A. P., Piotto, G., Renzini, A., et al. 2017, MNRAS, 464, 3636
Mucciarelli, A., Dalessandro, E., Massari, D., et al. 2016, ApJ, 824, 73
Nardiello, D., Libralato, M., Bedin, L. R., et al. 2016, MNRAS, 455, 2337
Nardiello, D., Milone, A., Piotto, G., et al. 2015a, A&A, 573, 70
Nardiello, D., Piotto, G., Milone, A. P., et al. 2015b, MNRAS, 451, 312
Ness, M., Asplund, M., & Casey, A. R. 2014, MNRAS, 445, 2994
Olech, A., Kaluzny, J., Thompson, I. B., et al. 2001, MNRAS, 321, 421
Ortolani, S., Barbuy, B., Bica, E., Zoccali, M., & Renzini, A. 2007, A&A, 470, 1043
Ortolani, S., Cassisi, S., & Salaris, M. 2017, Galax, 5, 28
Paust, N. E. Q., Reid, I. N., Piotto, G., et al. 2010, AJ, 139, 476
Pietrinferni, A., Cassisi, S., Salaris, M., & Castelli, F. 2004, ApJ, 612, 167
Pietrinferni, A., Cassisi, S., Salaris, M., & Castelli, F. 2006, ApJ, 642, 797
Piotto, G., King, I. R., Djorgovski, S. G., et al. 2002, A&A, 391, 945
Piotto, G., Milone, A. P., Bedin, L. R., et al. 2015, AJ, 149, 91
Planck Collaboration 2016, A&A, 594, A13
Recio-Blanco, A., Rojas-Arriagada, A., de Laverny, P., et al. 2017, A&A, 602, L14
Roediger, J. C., Courteau, S., Graves, G., & Schiavon, R. P. 2014, ApJS, 210, 10
Rojas-Arriagada, A., Recio-Blanco, A., de Laverny, P., et al. 2017, A&A, 601, A140
Rojas-Arriagada, A., Recio-Blanco, A., Hill, V., et al. 2014, A&A, 569, 103
Saracino, S., Dalessandro, E., Ferraro, F. R., et al. 2015, ApJ, 806, 152
Saracino, S., Dalessandro, E., Ferraro, F. R., et al. 2016, ApJ, 832, 48
Sarajedini, A., Bedin, L. R., & Chaboyer, B. 2007, AJ, 133, 1658
Schiavon, R. P., Johnson, J. A., Frinchaboy, P. M., et al. 2017, MNRAS, 466, 1010
Sirianni, M., Jee, M. J., & Benítez, N. 2005, PASP, 117, 1049
Soszyński, I., Udalski, A., Szymański, M. K., et al. 2014, AcA, 64, 177
Terndrup, D. M., Popowski, P., Gould, A., et al. 1998, AJ, 115, 1476
Testa, V., Corsi, C. E., Andreuzzi, G., et al. 2001, AJ, 121, 916
Trager, S. C., King, I. R., & Djorgovski, S. 1995, AJ, 109, 218
Valenti, E., Ferraro, F. R., & Origlia, L. 2010, MNRAS, 402, 1729
VandenBerg, D. A., Bergbusch, P. A., & Dotter, A. 2012, ApJ, 755, 15
VandenBerg, D. A., Brogaard, K., Leaman, R., & Casagrande, L. 2013, ApJ, 775, 134
Villanova, S., Moni Bidin, C., Mauro, F., Munoz, C., & Monaco, L. 2017, MNRAS, 464, 2730
Wagner-Kaiser, R., Sarajedini, A., & von Hippel, T. 2017, MNRAS, 468, 1038
Wagner-Kaiser, R., Stenning, D. C., Sarajedini, A., et al. 2016, MNRAS, 463, 3768
Wehlau, A., & Butterworth, S. 1990, AJ, 100, 686
Zoccali, M., Cassisi, S., Piotto, G., Bono, G., & Salaris, M. 1999, ApJL, 518, L49
Zoccali, M., Vasquez, S., Gonzalez, O. A., et al. 2017, A&A, 599, 12